Heterogeneous Dynamics and Polymer Plasticity

Alain Dequidt, Luca Conca, Jean-Yves Delannoy, Paul Sotta, François Lequeux, Didier R Long

Heterogeneous dynamics and polymer plasticity

Alain Dequidt[1], Luca Conca[2], Jean-Yves Delannoy[2],

Paul Sotta[2], François Lequeux[3], and Didier R. Long[2*]

(1) Institut de Chimie, Université de Clermont-Ferrand, F-63000 Clermont-Ferrand

(2) Laboratoire Polymères et Matériaux Avancés, UMR 5268 CNRS/Solvay,

85 avenue des Frères Perret, F-69192 Saint-Fons

(3) École Supérieure de Physique et de Chimie Industrielles de

la Ville de Paris (ESPCI) ParisTech, PSL Research University,

Sciences et Ingénierie de la matière Molle, CNRS UMR 7615,

10, Rue Vauquelin, F-75231 Paris Cedex 05, France

(Dated: April 3, 2017)

Abstract

We extend a model that has been proposed for describing mechanical properties of glassy polymers and which takes into account the heterogeneous nature of the dynamics. We describe their non-linear mechanical properties, up to a few 10% deformation. We propose that the elastic energy stored in the volume $\sim \xi^3$ of dynamical heterogeneities effectively reduces the free energy barriers present for internal relaxation. It allows to calculate yield stresses of order a few 10 MPa which are consistent as compared to experimental data without additional adjustable parameters than the scale ξ. The model is solved in 3D by numerical simulations with spatial resolution the scale of dynamical heterogeneities. We show that the prediction of pour model as regard to yield behavior are consistent with the value of $3-5$ nm for the scale for dynamical heterogeneities. Yield appears as the result of an acceleration of the dynamics of subunits with intermediate relaxation times which relax under stress before subunits with very long relaxation. Our simulations describe the onset of plastic behavior and the reorganization at the scale of dynamical heterogeneities. We predict the appearence of shear bands on a scale of a few tens of nanometers at yield and beyond.

* didier.long-exterieur@solvay.com

I. INTRODUCTION

A defining feature of polymers close to and below the glass transition is their mechanical properties. When temperature decreases from $T_g + 20$ K down to $T_g - 20$ K, the elastic modulus increases from typically 10^5 up to a few 10^9 Pa [1] and the dissipative modulus increases from a low value, which depends of the polymer details, up to 10^8 Pa, typically. Usually, the glass transition temperature T_g is defined as the temperature at which the monomer relaxation time reaches 10^2 s [2]. An important feature of glass transition is the strongly heterogeneous nature of the dynamics close to T_g [3, 4]. This strongly heterogeneous nature has been demonstrated experimentally over the past twenty years using NMR [5–7], fluorescence recovery after photo-bleaching (FRAP) [8–12], dielectric hole-burning [13] or solvation dynamics [14]. The characteristic size ξ has been estimated by NMR [6] to be 3 to 4 nm at $T_g + 20$ K (in the case of van der Waals liquids), whereas it is as small as 1 nm in glycerol [7].

Of high importance also are the plastic properties of glassy polymers. When applying a deformation below T_g, a yield stress is observed at a deformation amplitude of a few percents, which corresponds to a peak in the stress-strain curve. Beyond the yield stress, the stress displays a plateau at a value slightly lower than the peak: the polymer undergoes plastic flow. At deformations larger than about a few 10 %, strain hardening is observed in some cases, in particular for high molecular weight entangled or cross-linked polymers. These properties have been studied for many years, due their high practical importance [15]. The oldest model for describing plastic deformation is the Eyring model, which describes a bias motion under the applied stress. This effect is controlled by the so-called activation volume v, which is an adjustable parameter without clear interpretation [16, 17]. The idea that plastic flow results from a stress-induced acceleration of the dynamics at the molecular level is supported by several recent experiments [18–23]. Loo et al [18] have studied the dynamics in the amorphous phase of polyamide under stress by NMR. Kalfus et al [22] have studied dielectric relaxation during plastic flow. They observed that secondary relaxations are not significantly affected during deformation, whereas the α-relaxation is modified : an increase of $\tan\delta$ is indeed observed in the low frequency domain. Lee et al [19, 21] and Bending et al [20] have shown that small probe diffusion accelerates, and that the so-called stretching exponent β increases, under applied deformation. They interpreted this result by the fact that the dynamics becomes faster and more homogeneous during plastic deformation. In the case of polycarbonate with a T_g close to 423 K, Perez-Aparicio et al [23] have shown that the dielectric spectrum at room temperature, *i.e.* much below T_g, superimposes upon deformation to

the dielectric spectrum at rest slightly below T_g (depending of the strain rate), at least for the part of the spectrum accessible with their set-up.

From experiments it is known that internal stress can correspond to about one half of the mechanical energy in simple loading experiments [24]. This behavior has been recognized as a signature of dynamical heterogeneities in glassy polymers.

Mechanical properties of glassy polymers have been also studied by molecular dynamics (MD) simulations [25–31]. In particular, Leonforte et al [27] and Riggleman et al [25, 28] have shown that mechanical properties are heterogeneous. When submitted to an applied strain, the deformation field is non affine. Riggleman et al have shown that the elastic modulus is heterogeneous on a scale of order 1 nm, with some regions possibly showing negative moduli. The possible link between dynamical heterogeneities and these mechanical heterogeneities has been discussed in [32]. The idea that stress enhances molecular mobility is supported by these simulations. This idea has also been considered by Chen and Schweizer within the Non-linear Langevin equation model (NLE) [16, 17, 33–35]. Their model allows reproducing many features of plastic deformation. Even though these studies support the idea that the dynamics is enhanced during plastic deformation, a detailed description of the dynamical behavior from the molecular level up to the scale of a few tens of nanometers during plastic deformation is still missing. Besides, some of these approaches are mean field theories, which lack a spatial description.

The aim of this manuscript is to extend a model, in which a spatial description of dynamical heterogeneities on a meso-scale has been proposed, to the case of plastic deformation. This model had been initially developed in order to interpret both thin film experiments and the heterogeneous dynamics in the bulk [36–39], in van der Waals liquids and polymers. According to this model, the dynamics in the bulk is controlled by the percolation of slow domains, or subunits, corresponding to upwards density fluctuations on the scale of a few nanometers. It provides an expression for the characteristic size $\xi(T)$ of the heterogeneities, equivalently expressed as a number of monomers $N_c(T)$. The key feature for determining this size is a "Facilitation Mechanism".

The idea of facilitation is an old concept (see the review by Ritort and Sollich [40] and references therein) which has been also discussed more recently by Chandler and Garrahan [41, 42]. The idea is that the mobility at some point may be influenced and accelerated by a fast mobility of the local environment. A similar idea has been proposed by Merabia and Long [37], with an explicit mechanism. In this picture, facilitation results from free volume diffusion. The mecha-

nism proposed by Merabia and Long has been coined "Facilitation Mechanism" by Chen et al in their review paper in 2009 [43]. It has long been proposed that α-relaxation is a collective effect which takes place on a cooperative scale ξ [44]. Merabia and Long have proposed in [37] that this length scale results from distinct relaxation mechanisms in competition: 1) internal reorganisation within a slow subunit *at fixed free volume fraction*; 2) free volume diffusion from neigbhoring faster subunits. The competition between these two processes, which leads to a so-called 'facilitation mechanism' [43], results in a dominant length scale ξ of order $3-5$ nm close to T_g [37, 45].

This mechanism has been used also by Tito et al. for calculating mobility diffusion in suspended films [46]. The size ξ is a decreasing function of temperature and is found to be typically a few hundreds-one thousand of monomers close to T_g and a few tens at $T_g + 80$ K [37, 45]. This so-called "Percolation of Free Volume Distribution" (PFVD) model [43] provides a unified mechanism regarding various features of the dynamics in non-polar polymers close to the glass transition [43, 47, 48], such as the heterogeneous nature of the dynamics [36], the violation of the Stokes law observed for small probes [37], ageing and rejuvenation phenomena [45], the shift of glass transition at interfaces [32, 36, 38] and the dependence of the dynamics as a function of pressure [49]. In particular, the existence of broad distributions of relaxation times is supported experimentally by dielectric spectroscopy [4].

In a recent extension of this model [32], the stress and strain fields are described on the scale of dynamical heterogeneities. Macroscopic time scales and spatial scales of a few tens of nanometers can be reached. In the present manuscript, the plastic flow in glassy polymers is described with the same resolution. We focus on the onset of plastic flow, up to a few tens of percent of deformations, before the so-called strain hardening regime takes place [24]. This regime, which involves more specific polymer behavior, will be the focus of another paper. Note that a possible microscopic origin of strain hardening has been proposed by Chen and Schweitzer [35]. A main focus of our description is the spatial modification of the distribution of relaxation times by the applied strain and the ensuing relaxation processes. In particular, we show that plastic events are correlated, which results in shear bands on the scale of order 10 nm.

The manuscript is organized as follows. In section **II** we present the main modification of the physical model proposed in this manuscript in order to take non-linear effects into account, as compared to the description discussed in [32]. In this section, we show semi-quantitatively that, knowing or assuming the value of the scale ξ of dynamical heterogeneities, this model allows for calculating the yield stress without any additional adjustable paramaters. In section **III** we present

the numerical model which we have developed in order to solve the physical model. Note that this numerical model was already described in [32]. We refer to this article for further details regarding the physical model and the numerical model, as well as to [50] regarding the numerical model and the way it is solved. In section **IV** we describe the plastic behavior of glassy polymers as calculated from the numerical model, as regards the macroscopic behavior, *e.g.* yielding as a function of temperature or strain rate. In sections **V** and **VI** we analyse the physical mechanisms which take place at a scale of a few nanometers during plastic deformation, in particular the modification of the relaxation time distribution as compared to the linear regime, and the appearance of shear bands.

II. DESCRIPTION OF THE MODEL: STRAIN-INDUCED ACCELERATION OF THE DYNAMICS

The physical ingredients of the model are described in this section. For more details, the reader is refered to [32] and references therein. The underlying assumption of the model is that a wide distribution of relaxation times is created by density fluctuations on scale $\xi \sim 3 - 5$ nm [37, 45]. Each dynamical heterogeneity at the scale ξ is described by a high frequency elastic modulus $G'_0 \sim 10^9$ Pa and a local relaxation time. Entangled or cross-linked polymers also have a low frequency modulus of order 10^5 Pa. The model is schematized in Figure 1, in which subunits with different relaxation times are represented. A similar picture has been given in Merabia et al [38] and in Dequidt et al [32]. Mechanical experiments do not probe the internal relaxation times of the slower subunits because they relax the stress according to the faster relaxation times of their neighbors.

It is due to the fact that very slow subunits are rare. They are surrounded by faster subunits. Thus the local stress relaxes not according to the local internal relaxation time of the slow subunits, but according to the internal relaxation time of the fastest surrounding subunits. This issue is at the core of the percolation picture of the model and has been discussed in detail in Masurel et al [51].

A. Yield mechanism within the PFVD model

It is experimentally known that relaxation at a rate faster than the equilibrium rate τ_α^{-1} can be induced when a stress large enough is applied on a glassy material [15]. This implies that

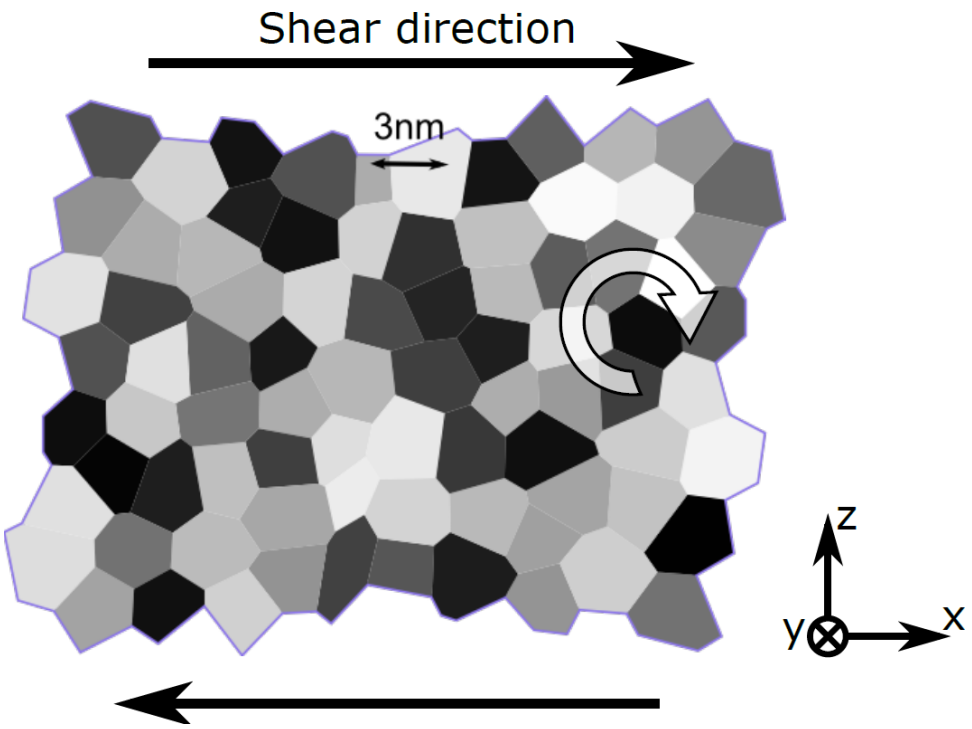

FIG. 1. Mesoscale model for polymers close to T_g. Subunits ($\xi \sim 3-5nm$) with different relaxation times are represented. Fast subunits are colored in white, slowest subunits in black. The elastic energy stored in slowest subunits does not relax by internal slow processes, but by rotation within a faster environment. The time scale of this final rotation may be set by the unperturbed distribution of relaxation times, or may be accelerated by yield mechanisms of surrounding subunits.

the local relaxation time cannot be a function of the local density only, but must also depend on the local stress. We assume that on a microscopic scale, the relaxation time follows an Eyring-like picture. For an elementary relaxation motion, one dynamical subunit has to overcome a free energy barrier $\Delta F_0(T)$, so that the relaxation time τ_α is given by $\tau_\alpha(T) = \tau_0 \exp(\Delta F_0/T)$, where τ_0 is a microscopic time of order 10^{-12}s corresponding to the time scale between collisions of neighboring monomers. T is the temperature expressed in Joule. Typically, $T \sim 4-5\times 10^{-21}$ J. According to the free volume picture, the α-relaxation process results from the packing of $N_c = \xi^3/a^3$ monomers, so that a volume of order a^3 (the monomer volume) is made available for one particular monomer to move (see *e.g.* reference [52]). This packing of N_c monomers results in an increase of the average free energy δf_0 *per monomer*. At rest, the overall free energy barrier for the α-relaxation is thus $\Delta F_0 = N_c \delta f_0$ (which is of order $30T$ close to T_g). When a stress is applied, the excess free energy per monomer during packing is modified into $\delta f_0 - \sigma^2 a^3/2G_0'$ where σ is the local (deviatoric) stress tensor and G_0' the high frequency storage modulus. At the scale ξ of dynamical heterogeneities, the

free energy barrier is thus modified into $N_c(\delta f_0 - \sigma^2 a^3/2G_0') = N_c\delta f_0 - \sigma^2\xi^3/2G_0'$. The activation energy $\Delta F = N_c\delta f$ for a local change of configuration (α relaxation) thus decreases as:

$$\Delta F = \Delta F_0(T) - \frac{\xi^3}{2}\frac{\sigma:\sigma}{G_0'} \tag{1}$$

In the absence of stress, each monomer is in a local free energy minimum. The position of each monomer fluctuates around the local minimum. For contributing to the α-relaxation process each monomer needs to undergo a fluctuation of free energy cost Δf_0. The collective coherent fluctuation for packing a number of order N_c monomers in order to create a hole of volume one monomer, costs thus $\Delta F_0 = N_c\Delta f_0$. Typically, at T_g, $\Delta F_0 \approx 30T$.

In the presence of a stress σ, each monomer is submitted locally to a force f which modifies its equilibrium position, before α-relaxation takes place on a longer time scale. In a one-dimensional picture, let us denote by X the position of a given monomer. $X = 0$ corresponds to the equilibrium position in the absence of applied stress. The position fluctuates in a potential well with stiffness k. When submitted to an external force f, one may calculate the Gibbs free energy in the presence of this applied force: $G(X) = -fX + kX^2/2$. The new minimum of Gibbs free energy corresponds to $dG(X)/dX = 0$, which reads $X_{eq} = f/k$ corresponding to an equilibrium position in the presence of the applied stress. It corresponds to a position with an increased free energy F by an amount $f^2/2k$ as compared to the position of the monomers without the presence of an applied stress. Expressed as a function of the applied stress and the elastic modulus, the increased free energy is $\Delta f_\sigma = \sigma^2 a^3/2G_0'$. The monomer positions fluctuate now around a new free energy minimum, in a potential well of the same stiffness as the initial one (red curve versus blue curve in Figure 2). The amplitude of the coherent fluctuations required for allowing for α-relaxation have been reduced by the same amount and is now $\Delta f_0 - \Delta f_\sigma$. This is exemplified in Figure 2 of the manuscript.

We assume that under the applied stress, each monomer can take its new equilibrium position in a time scale much shorter than the time scale required for the α-relaxation, because this new position results from individual and independent motions. On the other hand, α-relaxation takes place when a number of order N_c

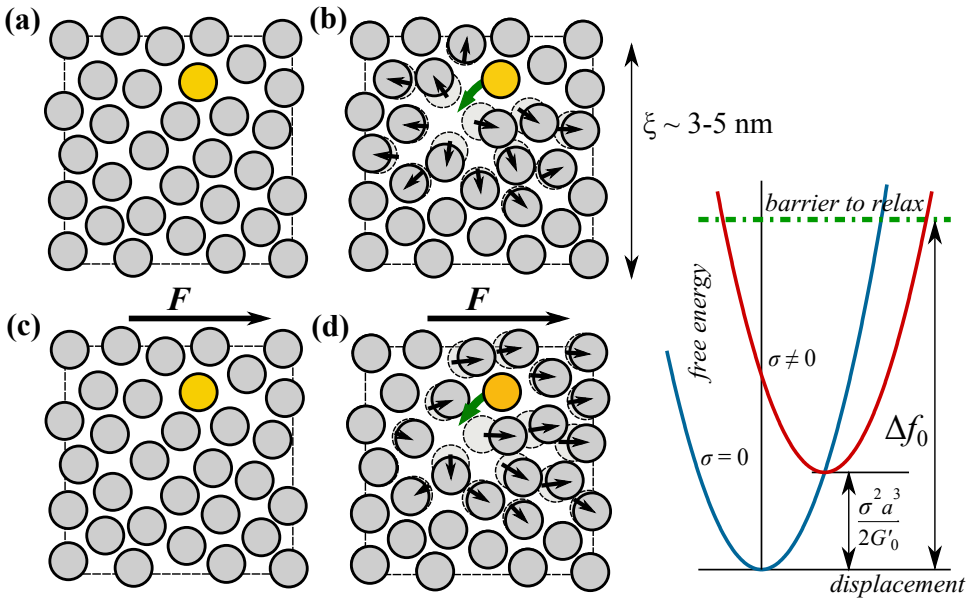

FIG. 2. (a) and (b):Schematics of α-relaxation. In the absence of stress, relaxation takes place by rearranging free volume on the scale ξ, *i.e.* by compacting about N_c monomers so as to create a hole of volume a^3, which is the volume of one monomer. This process has a free energy cost ΔF_0. (c) and (d): in the presence of an applied stress, there are some rearrangements on time scales shorter than the α-relaxation process which result in a lowering of the free energy barrier as discussed in the text. **The position of the monomer fluctuates then in a well of stiffness k (G_0') around this new equilibrium position (red curve).**

monomers fluctuate coherently in order to make a hole of volume one monomer, which is a very rare event. There is thus a separation of time scales between the equilibration of each of the monomers positions and the α-relaxation.

The free energy barriers has been lowered as it is cartooned in Figure 2.

The quantity σ:σ defined as

$$\sigma{:}\sigma = \frac{1}{2}\left[(\sigma_1-\sigma_2)^2+(\sigma_2-\sigma_3)^2+(\sigma_3-\sigma_1)^2\right] \tag{2}$$

where $\sigma_1, \sigma_2, \sigma_3$ are the eigenvalues of σ. σ:σ has been chosen because it is the only stress tensor-dependent quantity which is quadratic, invariant by rotation and vanishes at zero when stress is zero. Note that all quantities in this theoretical model, such as ξ, a, G_0', are known within a pre-factor of order unity, which need to be adjusted when comparing to experimental data. Local relaxation time are then accelerated according to

$$\tau(\sigma) = \tau_\alpha(T)\exp\left(-\frac{\xi^3}{2\,T}\,\frac{\sigma:\sigma}{G_0'}\right) \tag{3}$$

where $\tau_\alpha(T)$ is the relaxation time in the absence of stress. In the linear regime, when $\sigma{:}\sigma \ll {\sigma_c}^2 = 2T\,G'_0/\xi^3$, $\tau(\sigma) \approx \tau_\alpha$ and the equilibrium distribution of relaxation times is not modified.

Conversely, in the non-linear regime, when the local stress becomes high, i.e. when

$$\sigma{:}\sigma \sim {\sigma_c}^2 = 2T\,G'_0/\xi^3 \tag{4}$$

or equivalently $\xi^3\sigma{:}\sigma/(2T\,G'_0) \sim 1$, the distribution of relaxation times starts to deviate from equilibrium and mechanical rejuvenation is induced. Let us estimate the value of σ_c at this change of regime. Using $2T \approx 10^{-20}$ J, $G'_0 \approx 3 \times 10^9$ Pa, $\xi^3 \approx 10^{-25}$ m^3 (which corresponds to $\xi = 5$ nm) gives a typical value of a few 10^7 Pa for occurrence of stress induced softening (yield stress), obtained without any additional adjustable parameter. Equations (1) and (3), which account for the effect of the local stress on the relaxation time, are the main theoretical extensions to the model described in [32]. Their consequences are studied in this manuscript. Numerical simulations designed to solve the model are introduced in Section **III** and results are described and discussed in Sections **IV** to **VI**. However, let us first consider a simple mean field calculation of the yield stress.

B. Comparison with the classical Eyring picture

The interpretation for plastic flow proposed in this manuscript is qualitatively different from the classical Eyring's picture [53]. In the Eyring's model, the applied stress does not affect free energy barriers, but biases diffusion of monomers (or molecules in a simple liquid). The reference energy level in the direction of (resp. opposite to) the applied stress is decreased (resp. increased) by an amount $\delta E = \sigma v$, where v is the so-called Eyring activation volume. Assuming an activation barrier ΔF_0 between two consecutive states, the flux (shear rate) is given by

$$\dot{\gamma} = \frac{1}{\tau_0} \exp\left(-\frac{\Delta F_0}{T}\right) \sinh\frac{\sigma v}{T} \tag{5}$$

where τ_0 is a microscopic time of order 10^{-12} s and $\tau_\alpha = \tau_0 \exp(\Delta F_0/T)$ is the time associated to monomer or molecule diffusion in the absence of stress. Typically, ΔF_0 is of order 30 T close to T_g. In the linear limit where the applied stress is very small, the viscous flow is obtained by linearizing $\sinh(\sigma v/T)$ in equation (5), which gives

$$\dot{\gamma} = \frac{1}{\tau_0}\frac{v\sigma}{T} \exp\left(-\frac{\Delta F_0}{T}\right) \tag{6}$$

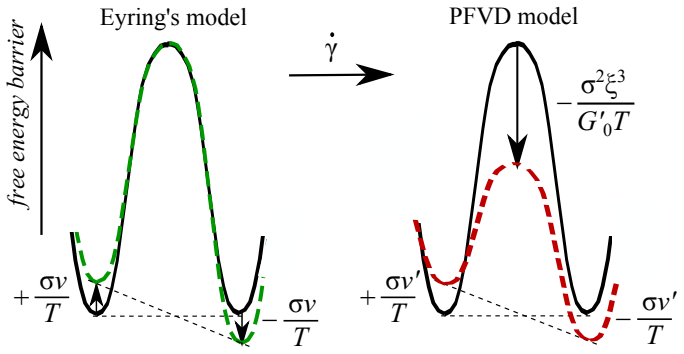

FIG. 3. The effect of local stress on the free energy activation barrier of the main polymer relaxation, in the presence of a shear rate $\dot{\gamma}$. While in the Eyring's model, the barrier is biased, in the model described here (denoted as PFVD model), the barrier is both biased and decreased. The barrier becomes significantly lowered at $\sigma = \sigma_c$.

The viscosity $\eta = \sigma/\dot{\gamma}$ is thus

$$\eta = \frac{T}{v}\tau_0 \exp\left(-\frac{\Delta F_0}{T}\right) \tag{7}$$

On the other hand, the viscosity is given by $\eta = G'_0\tau_\alpha = G'_0\tau_0 \exp(\Delta F_0/T)$. If there was only one relaxation time, the stress would relax at long times like $G'_0 \exp(-t/\tau)$, hence the relation $\eta = G'_0\tau$. In a dynamically heterogeneous liquids, it was argued in [36, 38] that there is a dominant relaxation time, τ_α which is essentially the 10% slowest part of the relaxation time spectrum and which dominates the long time part of the relaxation. A relation $\eta = G'_0\tau_\alpha$ is still valid though only within a prefactor of order unity [38]. By combining this relation with Equations (6) and (7), we obtain that the high frequency glassy modulus should be related to the activation volume by the relation $G'_0 = T/v$. The activation volume, determined when studying plastic flow, is usually found to be $v \sim 1$ nm^3 as we will see below, which gives $G'_0 \approx 4 \times 10^6$ Pa instead of 4×10^9 Pa typically. In the standard Eyring's model, there is thus an inconsistency of three orders of magnitude for describing both the plastic and linear regimes. This inconsistency needs to be resolved.

In the PFVD model introduced here, the applied stress not only biases the motion of monomers as it does in the standard Eyring's model, but, as discussed above, it also lowers free energy barriers, which the Eyring's model does not. This concept is schematized in Figure 3. In the PFVD model, when calculated in the same way as in the Eyring's model (Eq. 5) and using Eq. (1), the shear rate under applied stress σ is:

$$\dot{\gamma} = \frac{1}{\tau_0} \exp\left(\frac{-\Delta F_0}{T} + \frac{\sigma^2\xi^3}{2G'_0 T}\right) \sinh\left(\frac{\sigma v'}{T}\right) \tag{8}$$

The Eyring-like linear term $\sigma v'/T$ is necessary to bias the flow and to describe linear flows

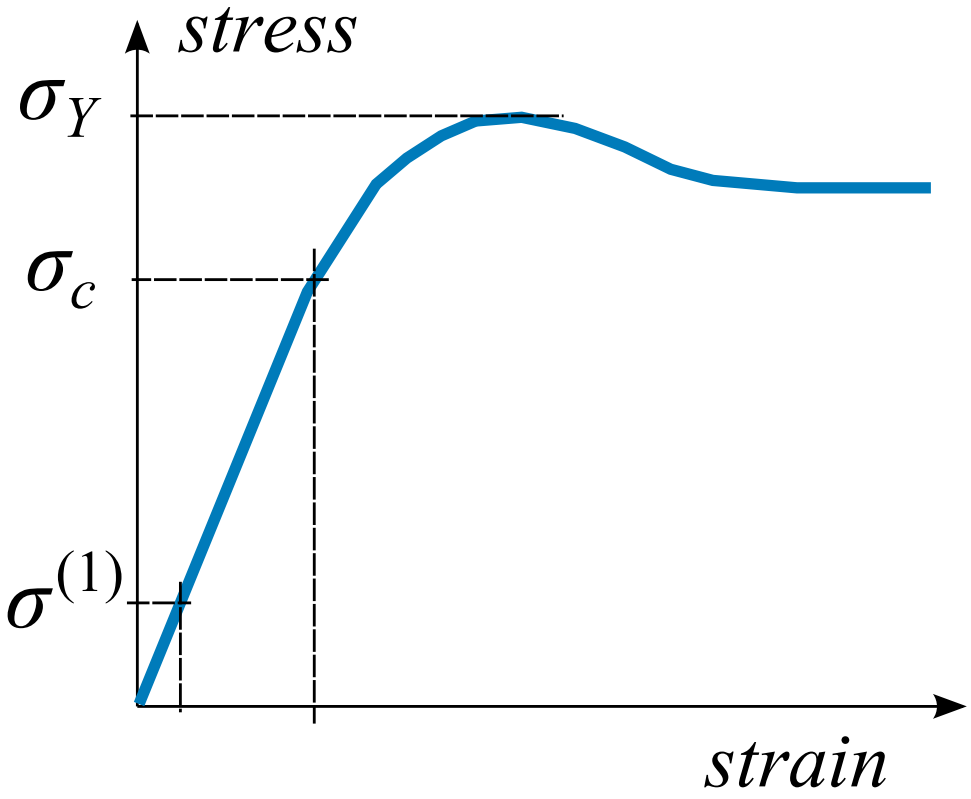

FIG. 4. We indicate $\sigma_c = (2G_0'T/\xi^3)^{1/2} \sim 10^7$ Pa which is the onset of plastic regime: the distribution of relaxation time starts to be modified by the applied stress. Typically, σ_c is of order 10^7 Pa. σ_y corresponds to the yield stress and is identified as the maximum on the stress-strain curve. Typically, σ_y is a few 10^7 Pa. $\sigma^{(1)}$ indicates a small stress value, within the linear response. Relaxation times are not affected by such small applied stress.

analytically. This term is dominant at very small stress. The volume v' is different from that of the Eyring's model. It satisfies the relation $v' = \frac{T}{G_0'} \approx 10^{-3}$ nm^3, which is typically three orders of magnitude smaller than the standard Eyring's activation volume v. On the other hand, as discussed above, plastic flow (yielding) is controlled by the quadratic term in the argument of Equation (8). Indeed, the non-linear regime initiates when the quadratic term in σ in argument in exp in Eq. 8 becomes larger than one. This corresponds to the threshold $\sigma \approx \sigma_c = (2G_0'T/\xi^3)^{1/2} \sim 10^7$ Pa. At $\sigma = \sigma_c$, the argument in the sinh of the right hand side of Equation 8, $v'\sigma/T$, is of order a few 10^{-3}. It follows that the non-linear regime is entirely dominated by the quadratic PFVD term. Yield stress is typically a few times larger than the critical stress σ_c which defines the onset of the non-linear regime. This is illustrates in Figure 4.

C. Connection between the PFVD model and the Eyring model

The obtained expression for plastic flow (Eq. 8) differs from that in the standard Eyring's model in two distinct ways. First, this is due to the term quadratic in σ in the argument of $sinh$ in Eq. 8. Secondly, in the PFVD model, the volume v' is three orders of magnitude smaller than usual v values measured experimentally within the Eyring picture. May these two points of view be reconciled ? As discussed above, in the classical Eyring's picture, the activation volume v is measured from the yield behavior. The effect of the applied stress on the distribution of relaxation times is generally not studied quantitatively, because experiments are difficult to perform in this regime [23]. Among experiments aimed at measuring the dynamics under imposed deformation, such as those in reference [19, 20, 54], the authors measured the evolution of a single characteristic time analogous to τ_α, associated to optical probe reorientation dynamics. Though they discuss the evolution of the width of the distribution of relaxation time thanks to a Kolhrauch coefficient characterizing the relaxation at long times, they do not have a direct access to the distribution of relaxation times. Kalfus et al and Perez-Aparicio et al [22, 23] aimed at measuring the distribution using dielectric spectroscopy, but only a part of it was accessible in their experiments. On the other hand, experimental data on the evolution of the relaxation times at very small deformation, well below yield, do not allow for checking the validity of Eyring's law, and linear flow results indeed show that it is not valid. It is only verified for stresses beyond the non-linear regime, for stress values typically comprised between the critical stress σ_c and the yield stress σ_y. The yield stress σ_y is such that the dominant relaxation time given by $\tau = \tau_0 \exp\left(\Delta F_0/T - \sigma_y^2 \xi^3/(2G'_g T)\right)$ is of order $\dot{\gamma}^{-1}$, that is

$$\sigma_y = \left(\frac{2G'_0 T}{\xi^3}\left(\frac{\Delta F_0}{T} + \ln(\dot{\gamma}\tau_0)\right)\right)^{1/2} \tag{9}$$

This expression relates the parameters of the model, G'_0, ξ and ΔF_0 to the yield stress σ_c. Below T_g one has typically $\Delta F_0/T \sim 35-40$, $\ln(\dot{\gamma}\tau_0) \approx -25$, $\xi^3 \sim 10^{-25}$ m^3, $G'_0 \approx 3\times10^9$ Pa, $T \approx 4\times10^{-21}$J. This gives $\sigma_y \approx 5 \times 10^7$ Pa. Close to σ_y, the expression for the energy barrier can be linearized around σ_y:

$$\Delta F(\sigma) \approx \Delta F(\sigma_y) + (\sigma - \sigma_y)\frac{d\Delta F}{d\sigma}(\sigma_y) = \Delta F_0(T) + \frac{\sigma_y^2 \xi^3}{2G'_0} - \frac{\sigma \sigma_y \xi^3}{G'_0} \tag{10}$$

The quantity

$$v = \frac{\sigma_y \xi^3}{G'_0} \tag{11}$$

as given by Equations (9) and (11), has the dimension of a volume. It may be considered as the standard Eyring's activation volume as calculated from the PFVD model. Its numerical value is thus $v \approx 1 - 2$ nm^3, which is a typical value for glassy polymer plasticity. Note that v obeys

$$v = \left(\frac{\partial \sigma}{T \partial \ln \dot{\gamma}} \right)^{-1} \tag{12}$$

This is the standard relation used according to Eyring's picture for calculating the Eyring volume based on experimental data when measuring the stress as a function of $\dot{\gamma}$. The linearized free energy barrier in the vicinity of σ_y reads numerically, according to Equation 10 and the values of parameters quoted above:

$$\Delta F(\sigma) \approx 45T - v\sigma \tag{13}$$

At $\sigma = \sigma_y = 5 \times 10^7$ Pa, a value $\Delta F(\sigma_y) \approx 25T$ is obtained. This is consistent with the onset of plastic flow since this value of the free energy barrier corresponds to a relaxation time of order 1 s. Therefore, our model can be mapped on the standard Eyring's model by giving a physical interpretation of the activation volume. The model contains no additional adjustable parameter as compared to those used in the PFVD model to describe linear mechanical properties [32], T_g shifts in thin films and Stokes law violation [36, 37].

D. Self-consistent calculation for the yield stress

A more precise value for the yield stress than in Equation (9) can be obtained self-consistently by solving the following equation under plastic deformation:

$$\sigma = G_0' \, \dot{\gamma} \, \tau(\sigma) \tag{14}$$

where τ is the typical relaxation time during plastic flow and σ is the applied stress. Note that in Equation (14), the high frequency modulus G_0' is not modified by applied shear. The effect of the stress is entirely contained in the relaxation time. Similarly, considering the macroscopic elastic modulus $G(T)$, a decrease of the elastic modulus by several orders of magnitude is observed when crossing the glass transition temperature. However, the high frequency modulus G_0', which is of the same order of magnitude as the bulk modulus K, is essentially not affected by temperature. The main effect is the shift of relaxation time distributions towards high frequencies. This has been discussed in detail in Dequidt et al. [32]. Due to non-linear yield, the relaxation time decreases under stress (see Eq. 3):

$$\tau = \tau_\alpha \exp\left(-\frac{\sigma^2 \, \xi^3}{2 \, G_0' \, T} \right) \tag{15}$$

Combining with Eq. 14 and taking the logarithm, one gets

$$\sigma^2 = \frac{2\,G_0'\,T}{\xi^3}\left(\ln(\dot\gamma\,\tau_\alpha) - \ln(\frac{\sigma}{G_0'})\right) \approx \frac{2\,G_0'\,T}{\xi^3}\left(\ln(\dot\gamma\,\tau_\alpha) + \frac{1}{2}\ln(\frac{G_0'\,\xi^3}{2\,T})\right) \tag{16}$$

where the equation (17) was obtained by taking $\sigma \approx \sigma_c \approx (2G_0'T/\xi^3)^{1/2}$ and is valid for $\dot\gamma\,\tau_\alpha > 1$. In a range of a few decades, σ_c expressed as a function of $\ln\dot\gamma\,\tau_\alpha$ can be linearized as

$$\sigma = a + b\ln\dot\gamma\,\tau_\alpha \tag{17}$$

with

$$a = \left(\frac{G_0'\,T}{\xi^3}\ln\frac{G_0'\,\xi^3}{2\,T}\right)^{1/2} \qquad b = \left(\frac{G_0'\,T}{\xi^3}\right)^{1/2}\left(\ln\frac{G_0'\,\xi^3}{2\,k_BT}\right)^{-1/2} \tag{18}$$

Equation (17) is a classical feature of the yield of polymers (see *e.g.* [55]). It is just the linearization of equation (16), and is valid provided $\frac{1}{2}\ln(\frac{G_0'\xi^3}{2T}) \gg \ln(\gamma\dot\tau_\alpha)$. It has therefore a limited range of validity within our model, and derives from a self-consistent calculation. Note that a similar equation within the context of the Eyring model and its limited validity has been discussed in reference [17]. Chen and Schweizer argued that the coefficient a and b deduced from the Eyring model does not follow the right temperature dependence. The temperature dependence of a and b deduced from our model may be different from that deduced by using the Eyring model. We will discussed that in another manuscript. Equation 17 allows for making the connection between our model and with the literature which uses a similar equation. It is similar to that obtained within the standard Eyring's model, but with different coefficients. Indeed, taking a as the yield stress value, the activation volume T/b is exactly the one given by 11, which evidences the consistency of our approach. Assuming $G_0' \approx 3\times10^9$ Pa, $T \approx 4\times10^{-21}$J and $\xi^3 \approx 10^{-25}\mathrm{m}^3$ (which corresponds to $\xi \approx 5$ nm), we obtain $a \approx 6\times10^7$ Pa and $b \approx 2\times10^6$ Pa, which are typical values. With the parameter values used here, one would find $v \approx 2$ nm^3 whereas $\xi^3 \sim 100$ nm^3 close to T_g. Our prediction is that, apart from logarithmic corrections, $v \propto \xi^{3/2}$ (see Eq. 18). However, the orders of magnitude of v and ξ^3 are very differents.

Considering for example polystyrene, the evolution of the characteristic length scale ξ, as calculated in ref [37], is plotted in Figure 5. From the temperature dependence of ξ and the WLF law, the yield stress of polystyrene can be calculated. The stress during plastic flow as calculated

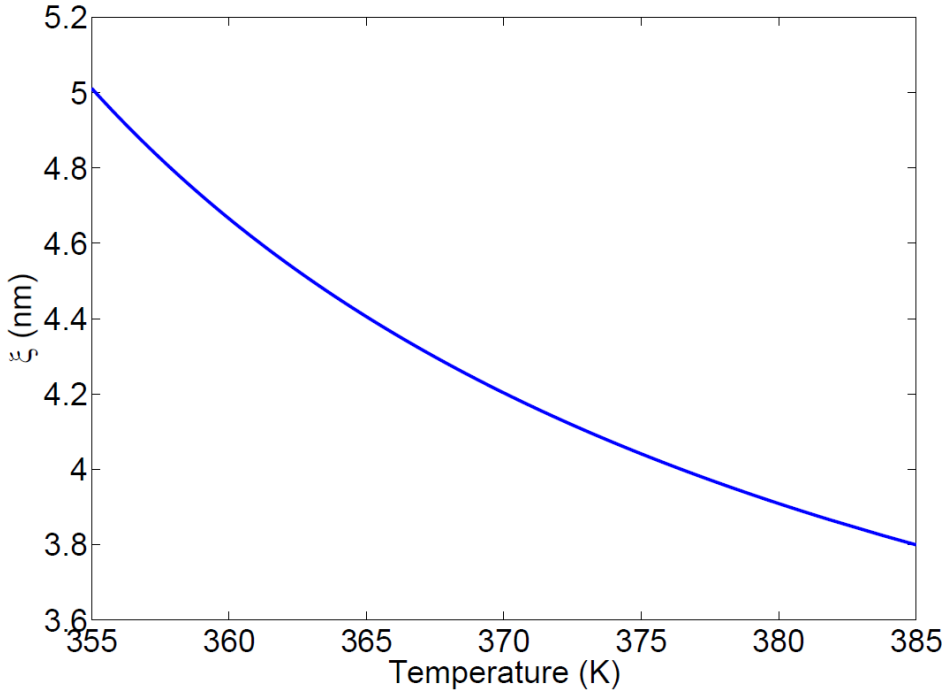

FIG. 5. Evolution of the length scale ξ of dynamical heterogeneities as a function of temperature, as calculated for polystyrene in ref [37].

from Equation 16 is plotted in Figure 6. The results are qualitatively consistent with experimental data, without additional adjustable parameter. The results from Figure 6 must be considered as qualitative. In particular, the approach to zero yield stress is only indicative. These curves are obtained from a self-consistent calculation in order to explain where the orders of magnitude come from. More quantitative results are obtained by numerical simulations further in the text. Note also that experimentally, the approach to zero yield stress is difficult to define since the overshoot tends to disappear. The relation $\sigma_y \approx K(T_g - T)$ relating yield stress to the temperature is approximately satisfied, with a slope which is consistent in order of magnitude with known experimental values, *i.e.* with $K \sim 10^6$ Pa K^{-1} [55, 56]. Note that the orders of magnitude are deduced from our model without new adjustable parameter as compared to earlier issues considered within the PFVD model. Plastic properties are essentially deduced from the value for N_c.

This phenomenological description amounts to consider that the elastic energy stored at the scale of dynamical heterogeneities is available for crossing internal free energy barriers in the liquid. No specific polymer effects have been taken into account yet, which limits the model to deformations of moderate amplitudes. Beyond deformations of about 20 %, effects such as strain hardening take

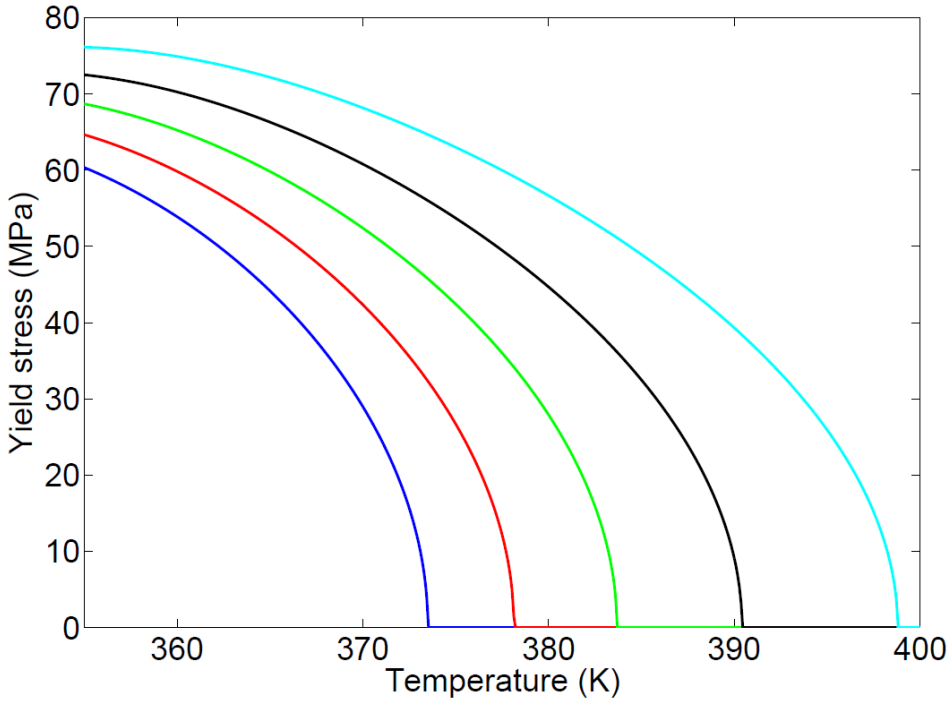

FIG. 6. Stress during plastic flow for polystyrene calculated according to Equation (16) and to the evolution of τ_α (WLF law) and ξ as a function of temperature (as shown in Fig. 5), for different strain rates: $\dot{\gamma} = 10^{-2}s^{-1}$ (blue curve), $10^{-1}s^{-1}$ (red curve), $1s^{-1}$ (green curve), $10s^{-1}$ (black curve), $10^{2}s^{-1}$ (turquoise curve)

place (see *e.g.* [57]). Taking them into account will require further extensions of the model. Let us consider now how the resolution of the model in 3D for calculating plastic flow at the scale of dynamical heterogeneities.

III. NUMERICAL MODEL

The basic units of the numerical model are dynamical heterogeneity subunits (of typical size $\xi \sim 3-5$ nm). They are represented by beads interacting through springs and hard core repulsion, which account for incompressibility.

Hard core repulsion between nodes is expressed by the force

$$\vec{f}_{ij}^{(rep)} = 12\ u_0 \left(\frac{d}{r}\right)^{12} \frac{\vec{R}_{ij}}{r^2} \tag{19}$$

with $\vec{R}_{ij} = \vec{R}_i - \vec{R}_j$, where $\vec{R}_i$ is the vector position of the center of bead i and $r = ||\vec{R}_{ij}||$. $\vec{f}_{ij}^{(rep)}$ is cut off and regularized at long range. u_0 is small enough so that its contribution of f^{rep} in shear measurements is negligible. $d \sim \xi$ scales the interactionr range

Rubbery elasticity of cross-linked or entangled polymers is modeled by very loose, permanent springs interacting with the force:

$$\vec{f}_{ij} = -k_\infty \left(r - l_0\right) \frac{\vec{R}_{ij}}{r} \tag{20}$$

k_∞ is the low frequency elastic constant corresponding to rubber elasticity. $k_\infty \sim G'_\infty \xi$ with $G'_\infty \approx 1$ MPa sets the unit of stress in the simulation. The length $l_0 \sim \xi$. The average number of glassy springs per node is an adjustable parameter of the numerical model. We took the same adjustable parameters as in [32] (see Table 1 in Appendix).

The heterogeneous dynamics is modeled by glassy springs with a high frequency elastic constant k_0 corresponding to the glassy modulus G'_0 and with finite relaxation times. The high frequency, glassy force between two neighboring beads is given by

$$\vec{F}_g \sim -k_0 \, \delta\vec{R}_{ij} \tag{21}$$

where k_0 is the high frequency elastic constant corresponding to the glassy modulus G'_0: $k_\infty \ll k_0$, and $\delta R_{ij} = \vec{R}_{ij} - \vec{R}^{\rm ref}_{ij}$. The reference state $\vec{R}^{\rm ref}_{ij}$ corresponds to the relative positions of the subunits when the last relaxation event occurred. The probability for breaking per unit time, dP/dt, is given by

$$dP \sim \frac{dt}{\tau_{\alpha,loc}(t)} \tag{22}$$

where $\tau_{\alpha,loc}(t)$ is the relaxation time of the glassy link at time t.

Simulated samples are 36 nm thick and are submitted to simple shear deformation. The values of the parameters we use in the numerical model are given in Appendix. All the details regarding the numerical model have been published in [32].

A. Relaxation and aging mechanism

When temperature changes, the equilibrium spectrum of relaxation times is shifted (possible broadening of the equilibrium spectrum upon cooling is neglected) according to the experimental WLF law of the considered polymer:

$$\log \frac{\tau_\alpha}{\tau_g} = \frac{-C_1 \left(T - T_0\right)}{C_2 + T - T_0} \tag{23}$$

where $\tau_g = 1$ s. This function is plotted in Figure 7 for the particular case of PMMA. The corresponding WLF coefficients are given in Table I. Parameters for PMMA, with $T_g = 393$ K, will

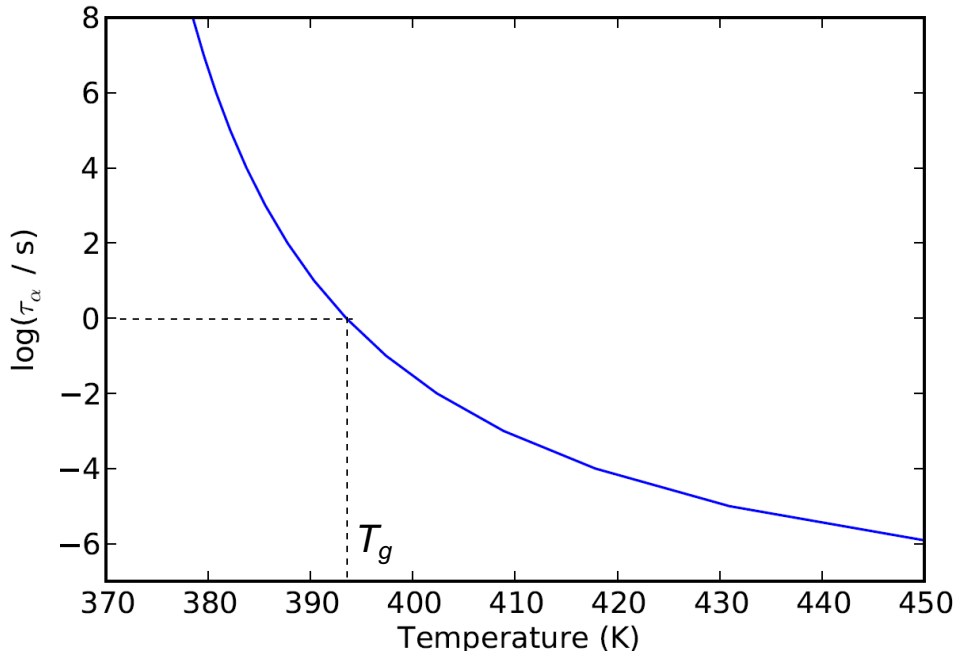

FIG. 7. Variation of the time shift factor with temperature for the distribution of relaxation times used in the simulations. It corresponds to the WLF law of PMMA, with $T_g = 393$K.

be considered in all what follows. We have chosen a log-normal distribution for the equilibrium distribution of relaxation times τ:

$$p_{eq}(\log(\tau)) \propto \exp\left(-\frac{\log^2 \frac{\tau}{\tau_\alpha}}{\Delta^2}\right) \tag{24}$$

where τ_α is the maximum of the distribution (of $\log \tau$) and Δ sets the width of the distribution (of log). The corresponding distributions of relaxation times are given in Figure 8. The width $\Delta = 4$ of the distribution has been chosen to be consistent with measured dielectric spectra and with measured temperature and frequency variations of G' and G'' [51, 68].

Broadband dielectric spectroscopy measurements in the temperature/frequency region of the glass transition show as well broad peaks of the loss permittivity ϵ", which can be qualitatively related to relaxation time distributions spanning typically 4 decades or more in some cases (see e.g. Richert [58] and numerous data compiled in chapter 7 of [59] (Figures 7.13 and 7.14 pages 250-251) and in Havriliak [60]. To provide a more definitive answer to this issue, detailed comparison would be required regarding simulation results and mechanical data, especially regarding the loss modulus, which is very sensitive to the width of the distribution of relaxation time.

In order to properly account for the local dynamics, the following scheme is used. At equilibrium, the distribution of rupture times should be identical to the distribution of relaxation times $p(\tau)$

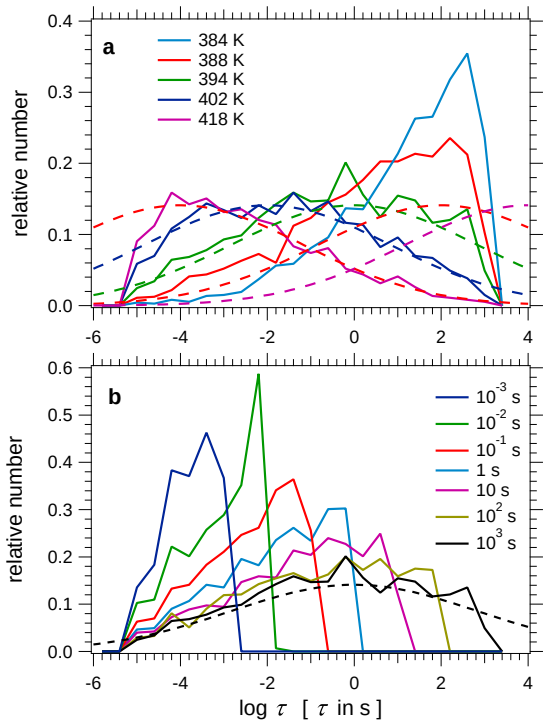

FIG. 8. (a): Distributions of relaxation times at rest for different temperatures between $T = 384$K and $T = 418$K. The system have aged at the considered temperature for 10^3s. The typical width of the distributions lay between 6 and 8 decades. Dashed curves corresponds to the equilibrium distributions at the considered temperatures given by Equation (24). (b): Distributions of relaxation times at different ages at rest, at $T = 394$K. Aging times vary from 10^{-3}s up to 10^3s. The dashed curve corresponds to the equilibrium distribution.

given by Equation (24). The age (the elapsed time since the last relaxation event) is recorded for each spring. Then, the rupture probability during a timestep $\mathrm{d}t$, that is the probability of not reaching the age $t + \mathrm{d}t$ knowing that the spring is aged t, can be calculated:

$$p_{rup}^{eq} = 1 - \frac{p(t + \mathrm{d}t)}{p(t)} \approx -\frac{\mathrm{d}\log p}{\mathrm{d}\tau}\bigg|_{\tau=t} \mathrm{d}t \tag{25}$$

p is the distribution of relaxation times at the given temperature. Note that we calculate two different quantities. The age of a spring, which is the elapsed time since it last underwent a relaxation event, and the relexation time of the spring. The corresponding distributions at equilibrium are the same. Here, due to the applied stress, both distribution are different: The stress reduces the relaxation time, even if no relaxation event takes place, whereas it does not modify the age, until a relaxation event takes place. This event, on average, will appear earlier as compared to the situation when no stress is present. In the following, we will discuss only ages distributions, which we denote "relaxation time distributions" for the sake of clarity because it is a more standard word.

For broad distributions of relaxation times like those we are considering, $p(\tau) \sim \frac{1}{\tau}$ over a wide range and Equation (22) reduces to $\tau_{\alpha,loc} \sim t$. Note that the distribution is very close to a $1/t$ law, up to a cut-off. The equilibrium distributions of relaxation times discussed by Merabia and Long [37, 45] , Dequidt et al. [32], or Masurel et al. [51] is essentially flat on a log scale -corresponding to the $1/t$ behavior, and decreases beyond a certain $\log \tau$ value which depends on temperature. In any case, the distribution given here by Equation (25) is integrable.

Both quenching (ageing) and annealing of glassy polymers can be modelled by the procedure described above [32]. As examples, we show relaxation time distributions of systems that were quenched (Fig. 8.a) at various temperatures and aged for 10^3 s, or that have aged at $T = 394$K for various waiting times (Fig. 8.b). The cut-off at long times in Figure 8 corresponds to the ageing time. In Fig. 8.a, all samples have aged for 10^3s. The distributions of relaxation times then have a cut-off at about the same time scale, as was discussed for instance by Merabia and Long [45]. In Fig. 8.b, one observes distributions with cut-off approximately equals to 10^{-3}s, 10^{-2}s, 10^{-1}s, 1s, 10s, 100 s and 1000 s, which corresponds approximately to their respective ageing times.

In the presence of an applied stress, the probability of rupture is modified as

$$p_{rup} = p_{rup}^{eq} \exp(\lambda \, \delta R^2) \tag{26}$$

This equation is a direct translation of Equation (2) of the physical model, when parameters values are mapped onto the numerical model. This equation expresses the fact that the local stress lowers the local free energy barrier for α-relaxation. The value of the parameter $\lambda \sim \xi G_0'/2T$ is taken to be $\frac{1000}{\xi^2}$, which is consistent with the estimation given in section II. Indeed, the argument in the exponential becomes of order one for a strain δR of order 3%. The numerical values of the parameters used in the model are reported in Appendix. We refer to Dequidt et al [32] for further details regarding the numerical model, and also to Merabia et al [50] wherein a very similar numerical model has been described in another context (filled elastomers).

IV. PLASTIC BEHAVIOR: YIELD STRESS

Let us first consider the evolution of the stress as a function of the strain amplitude for systems sheared at a constant shear rate $\dot{\gamma}$ (Fig. 9). At temperatures above T_g and at low shear rate, a linear variation of the stress, with a slope corresponding to the rubbery modulus of the polymer, is observed (Fig. 9.a). In the glassy regime, experimental stress-strain curves have a much larger slope at small deformation amplitudes, because the glassy elastic modulus is 3 orders of magnitude

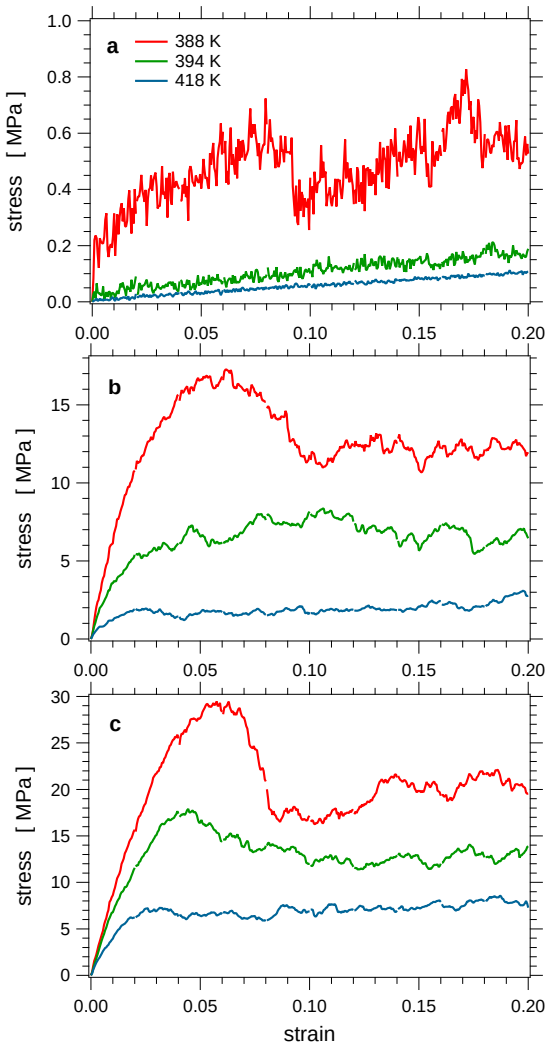

FIG. 9. (a): Stress-strain curves at various temperatures and at strain rate $\dot{\gamma} = 10^{-2}$ s^{-1}. At $T > T_g$, the stress increases linearly with the strain amplitude γ. Non-linear behavior is observed at temperatures close to and below T_g. (b) Same as (a), strain rate $\dot{\gamma} = 10^{-1}$ s^{-1}. At a given strain value, the stress is higher than in (a). (c): Same as (a) and (b), strain rate $\dot{\gamma} = 1$ s^{-1}. At a given strain value, the stress is higher than in (b).

larger than in the rubbery regime. The slope at small deformation is of order 1 GPa, as it should be. In addition, a maximum (yield stress) is generally observed experimentally, of typically a few tens of MPa at *e.g.* 20K or a few tens of Kelvins below T_g. An overshoot is indeed observed in Figures 9.b and 9.c at low temperatures.

Our interpretation is that the overshoot is the result of a retardation effect between the local relaxation time under stress and the effective relaxation event which is analogous to a Poisson

process for each subunits, and to the fact that relaxation events take place on a relatively limited time window around a critical deformation γ_y. Upon increasing deformation, the local relaxation times decrease and many subunits relax in relatively narrow time window for deformation close to γ_y corresponding to yield. If these relaxations took place more evenly on a broader time frame just after starting deformation, one would observe a monotonous increase of the stress until it reaches a plateau as a function of the strain amplitude (results not shown here). On the other hand, if these relaxation events take place in majority around γ_y, the stress drops because these slow subunits are replaced by faster ones and that the stress they bore relaxes suddenly. Note that according to this picture, one would observe a strain softening followed by damped oscillation for the stress if these relaxation events took place on a very restricted time frame. This is not the case because they are sufficiently uncorrelated for the ensuing relaxation to be over-damped. Thus, we interpret the overshoot and the strain softening regime as the consequence of a narrow, but not too narrow time window for initiation of the stress induced relaxation processes. Our point of view is that this is a similar process which happens in the calculation of Medvedev and Caruthers [61]. Note also that an overshoot is obtained within the NLE approach by Chen and Schweizer, resulting from the coupling between stress and dynamics [62].

It can be observed that the results of Figure 9 are noisy. This is due to the relatively small size of the numerical box (1000 particles), and also because local forces can be high as a consequence of the random relaxation of glassy springs. We do not consider the apparent non-monotonicity as significant.

A linear dependence is observed when the yield stress is plotted as a function of the logarithm of strain rate (Figure 10.a). This fact is one characteristic defining feature of glassy polymers [55]. Under the applied deformation, the relaxation is locally accelerated, according to Equation (3), and some slow subunits relax. The corresponding local stress is then transferred to surrounding non relaxed subunits, which are then more likely to yield non-linearly. The successive occurrences of local non-linear yield events make the global stress decrease and reach a quasi stationary value.

The yield stress is plotted in Figure 10.b as a function of the aging time (after a temperature quench). A linear dependence of the yield stress as a function of the logarithm of the aging time is observed. Note that in both Figures 10.a and 10.b the slopes depend only weakly on temperature. During ageing, τ_α evolves as a function of the waiting time t_w following the Struik's law

$$\tau_\alpha \sim t_w^\beta \tag{27}$$

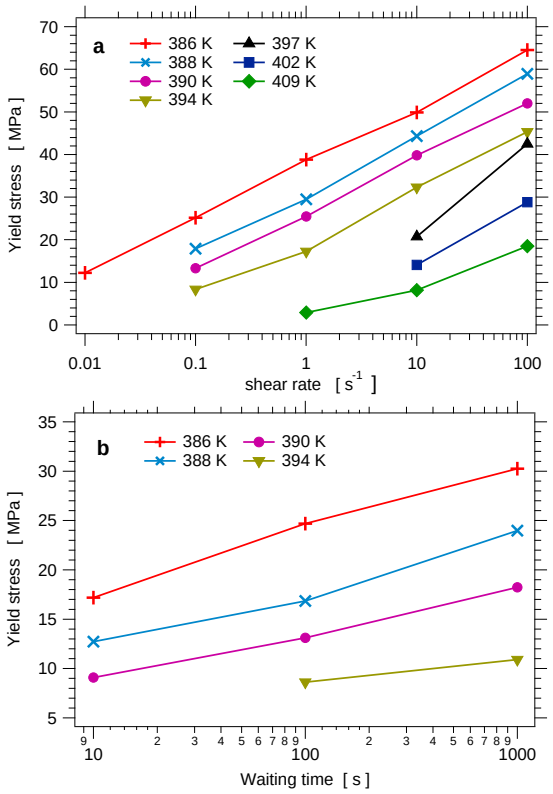

FIG. 10. (a): Yield stress as a function of the strain rate, at various temperatures between $T = 386$ K and $T = 409$ K and ageing time 100 s. A logarithmic dependence is observed. (b): Yield stress as a function of the ageing time before shearing, at various temperatures between $T = 386$ K and $T = 394$ K. The shear rate is 0.1 s^{-1}. The yield stress varies linearly with the logarithm of the ageing time. At temperatures higher than 394 K, no stress overshoot is observed. Note that in both cases, the lower the temperature, the higher the yield stress.

The slope in Figure 10.b is indeed lower than in Figure 10.a, which corresponds to an aging exponent β different from 1 (close to 0.6 in the simulations).

V. PLASTIC BEHAVIOR AND DISTRIBUTION OF RELAXATION TIMES

We consider here the modification of the relaxation time distributions induced by the distribution of local stress. This is a complex process, because the local stress is very heterogeneous. Indeed, it depends on the history of the deformation and internal relaxation processes, which themselves are stress dependent. The local stress in very slow subunits may also relax by a local individual relaxation when the neighboring subunits have relaxed according to their own relatively faster relaxation time: the stress in very slow subunits relaxes on the time scale of the relaxation

of its neighbors. Thus, the local relaxation time and stress are coupled in a complex way and are strongly history dependent [63].

These two mechanisms (spontaneous internal relaxation and relaxation of the surrounding subunits) allow local stress relaxation. To analyze these processes, we study in this section the evolution of the distribution of relaxation times as a function of strain amplitude in simple shear experiments up to deformation 0.3, for different temperatures (above and below T_g) and for different shear rates between 10^{-2} s^{-1} and 10^{2} s^{-1}. At high temperature, we expect that the relaxation time distribution is not modified by the applied deformation and remains that at equilibrium or after ageing. Upon decreasing temperature or increasing the shear rate, the applied deformation becomes too fast as compared to the initial relaxation times, the stress increases and the of relaxation time distribution gets modified. The cumulative distributions of relaxation times are plotted in Figure 11.a for different temperatures between $T = 388$ K and $T = 418$ K, at several increasing shear deformations, with $\dot{\gamma} = 10^{-1}$ s^{-1}. The distributions are indeed not modified by the applied shear at high temperatures ($T = 418$ K and $T = 402$ K). Conversely, the distributions are affected upon decreasing temperature. While the long time and short time parts of the distribution are not significantly modified, the strongest modification occurs for intermediate relaxation times, which is clearly visible on the $T = 388$ K bundle of curves. The cumulative distributions of relaxation times are plotted in Figure 11.b for various shear rates between 10^{-2} s^{-1} and 10^{2} s^{-1}, at $T = 394$ K, which is close to T_g. For the lowest shear rate (black bundle of curves), the cumulative distribution is not modified. At $\dot{\gamma} = 10^{-1}$ s^{-1}, the distribution is slightly modified. At the highest shear rate (red curves), the distribution is strongly modified for times shorter than 10^{-2}s.

Note that a stochastic model have been eveloped for studying the evolution of the relaxation time spectrum during cooling and heating [45] and also under applied strain [61]. These authors predict a shift of the relaxation time spectrum towards higher frequencies under strain similar to the evolution upon heating. Instead of a Fokker-Planck equation for calculating the evolution of the relaxation time distribution as proposed by Merabia and Long [45] and then by Medvedev and Caruthers [61], we calculate for each subunit a random evolution of the local relaxation time.

Both model presented here or the stochastic approach used by Mevedev and Caruthers [61] base their approach on a coupling between stress and dynamics. Applied stress accelerates the dynamics. However, the stochastic model used by Medvedev and Caruthers, or by Merabia and Long [45] cannot provide a detailed spatial distribution of the relaxation time. The stochastic approach is mean field in nature, and is inadequate for predicting the appearance of shear bands as it is the case in the present model, or more generally possible spatial correlation regarding

relaxation events. The random aspect in the model and simulation described in this manuscript is brought by the random process for relaxation events, and then, the spatial distribution of ages and local stress.

Thus, we do observe indeed that the distribution of relaxation times gets rejuvenated by shear at low temperatures or high shear rates, due to the non-linear breaking of the springs. Note that it has been observed experimentally that the mobility is accelerated in actively deformed polymers close to the glass transition [19]. Interestingly, the springs most sensitive to non-linear yield are not the oldest ones, but the ones of age similar to $\dot{\gamma}^{-1}$. Indeed, the long time parts of the bundles of curves remain narrow in all cases. This shows that stress does not accumulate in these springs although they do not break. Once all subunits surrounding a very slow subunit have released their stress by internal relaxation processes, the latter no longer bears stress: the local stress has relaxed. As a consequence, the non-linear acceleration of the dynamics is not effective for inducing internal relaxation of the very slow subunits because the surrounding subunits will always relax first. An example of a relaxation time distribution strongly modified by the applied deformation at the considered temperature and shear rate is plotted in Figure 12. Applying a stress induces a hole in the distribution of relaxation times around the time scale of the applied deformation. As a result, the distribution after shear is bimodal.

VI. REORGANIZATIONS UNDER STRAIN

Non affine reorganizations play a key role in yield mechanisms. The aim of this section is to quantify these non-affine reorganizations which result from the intrinsic heterogeneity (distributions of relaxation times) of the system. To quantify the non-affinity, the relaxed state just before the applied deformation is chosen as reference state. For a given bead, the non-affine displacement is defined at any time as

$$\delta\vec{r} = \Gamma^{-1}\vec{r} - \vec{r}_0 \tag{28}$$

where $\vec{r}_0$ is the initial (reference) position of the bead and $\Gamma^{-1}\vec{r}$ would be the affinely deformed current position of the bead in the reference system. The root-mean-square non-affine displacement is also defined by

$$d_{na} = \sqrt{\langle \delta\vec{r}^2 \rangle} \tag{29}$$

Brackets denote the average over all the beads. The evolution of d_{na} as a function of the strain γ is shown in Figure 13. d_{na} increases linearly at small strain. At high temperature (above T_g), it

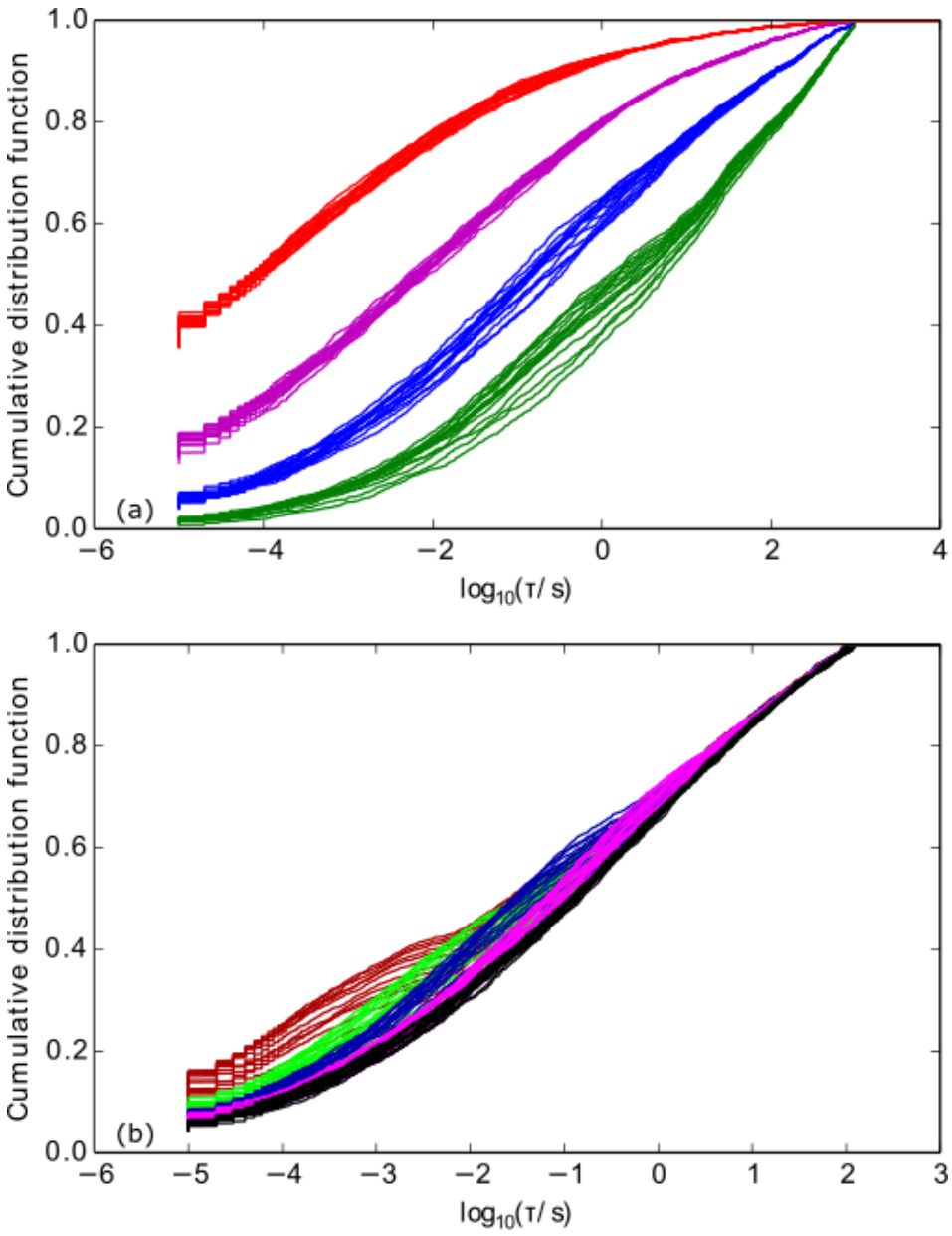

FIG. 11. Bundles of cumulative distributions of relaxation times. Each curve of a bundle corresponds to a given deformation, that is to a given time during the applied simple shear deformation. A bundle is made of these different curves for increasing deformations between 0 and 30 % (from bottom to top). A very narrow bundle corresponds to distributions which are not modified by the applied deformation. (a): Different temperatures are considered: $T = 388$ K (green curve); $T = 394$ K (blue), $T = 402$ K (purple); $T = 418$ K (red). Samples have aged for 10^3 s before deformation. The shear rate is $\dot{\gamma} = 10^{-1}\mathrm{s}^{-1}$. (b): $T = 394$ K, aging time 10^2s. Different shear rates $\dot{\gamma}$ are considered: $10^{-2}s^{-1}$ (black), $10^{-1}s^{-1}$ (purple), $1s^{-1}$ (blue), $10s^{-1}$ (green) and 10^2s^{-1} (red). At low shear rates or high temperatures, the bundles are narrow: the relaxation time distribution is not modified by the applied deformation. At high shear rates or low temperatures, the bundles increasingly broaden on the short time side: the distributions of relaxation times are modified by the applied deformation.

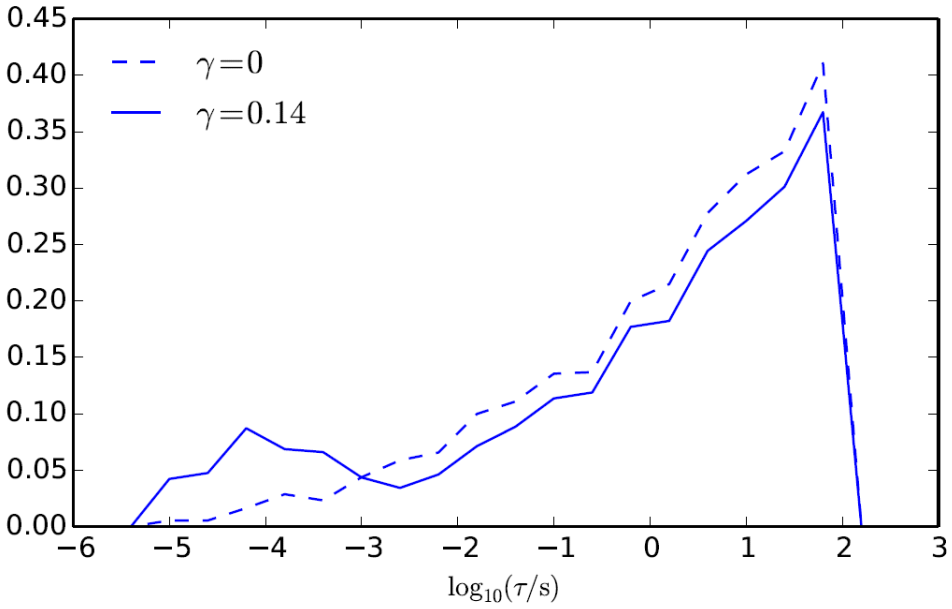

FIG. 12. Example of a distribution of relaxation times modified by the applied deformation. Aging time is 10^2s, shear rate $10^2\mathrm{s}^{-1}$, strain 14 % and temperature 386 K. The distribution of ages after shear is bimodal when the non-linear effect is significant. The behavior shown here is similar to the one observed for the cumulative distributions of relaxation times in Figure 11.a. The distribution is indeed affected in the intermediate range of relaxation times.

increases linearly for the whole deformation range. At temperatures close to or below T_g, a change of slope occurs at deformation 6-7 %, which corresponds to the yield point. Beyond this point, the lower the temperature, the larger the increase of d_{na} as a function of the applied deformation. Note that deformation is non-affine even in the linear regime of deformation. This is a generic feature of disordered elastic materials which has been dsicussed in detail in elastomers for instance by Long and Sotta [64–66]. In systems where the local elastic modulus is not uniform, the square of non-affine displacement at small deformation is proportional to γ^2 where γ is the amplitude of deformation. In a different context, Long and Sotta showed that the onset of plastic behavior corresponded to the change of slope of d_{na} as it is also the case here.

We also calculated the average velocity profile in the direction normal to the applied shear. The velocity profiles are plotted at different deformations for temperatures above T_g (Figure 14.a) and below T_g (Figure 14.b). The velocity profile is affine above T_g for the two considered snapshots (1 % and 7 % deformations respectively). Below T_g it is still affine at deformation 1% (elastic regime), whereas two shear bands are observed above the yield point at deformation 7 %. Note that in series of simulations performed in similar conditions (temperatures, strain rates, aging time), the

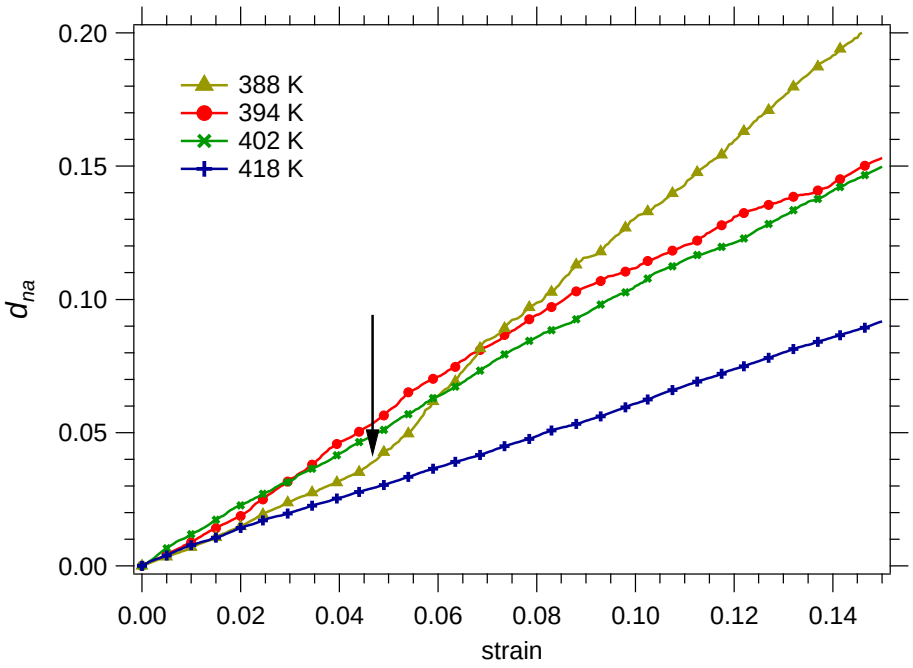

FIG. 13. Non-affine displacement d_{na} as a function of the strain amplitude for different temperatures. The shear rate is 0.1 s^{-1} and the waiting time is 100 s. d_{na} rises linearly with strain. Below T_g, the yield point is identified by a change of the slope: non-affine displacements are more pronounced in the plastic regime.

number of shear bands varied between 1 and 3. Thus, describing in detail the yield mechanisms at this scale would require a statistical analysis.

As discussed above, yield occurs when slow subunits (with relaxation time longer than the time scale t of the experiment) no longer percolates as their fraction has sufficiently decreased under the effect of the applied stress. Then could large reorganization length scales be observed under strain? To address this issue, we have calculated the spatial correlations of the non-affine displacement below, at and beyond yield. The spatial correlations of non-affine displacements in the x direction $\langle \delta x_i \, \delta x_j \rangle$ is calculated as the average over all i, j pairs in the same xy plane, separated by a distance $r = |\vec{r}_{0i} - \vec{r}_{0j}|$. The correlation function $\langle \delta x_i \, \delta x_j \rangle$ is plotted as a function of r in the inset in Figure 15. It decreases exponentially and a correlation length can be measured. This length is an estimate of the characteristic size of the clusters of beads which move more or less rigidly together. The correlation length is plotted as a function of the deformation γ in Figure 15. The following behavior may be expected. Some neighboring springs (in the xy plane) get additional stress while other ones (in the z direction) release some stress. Due to the non-linear effect, the neighboring springs for which the stress increases may break. A roughly planar region of broken springs, with low shear modulus, progressively appears, which is similar to a shear band. On

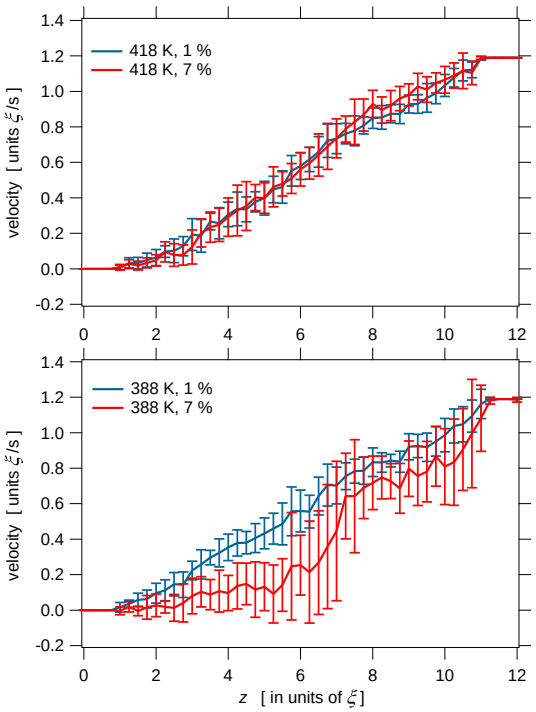

FIG. 14. (a): Velocity profiles as a function of z (normal to the flow) at temperature $T = 418$ K $\approx T_g + 25$K at 1 % and 7 % deformation. Error bars correspond to the standard deviation of bead velocities at a given altitude. The velocity profile remains essentially affine. (b): Same as in (a) but at temperature $T = 388$ K (below T_g). In the elastic regime (deformation 1 %), the velocity profile is essentially affine whereas at 7 % deformation, the velocity profile becomes non-affine. Three blocks moving rigidly separated by two shear bands can be observed.

both sides of this "crack", clusters of beads should be relatively little deformed and should move together. The correlation length should then be comparable to the typical size of the "cracks", which increases up to yield.

The appearance of shear band is due to the fact that when a subunit relax, the stress it bears is transferred to the next one, which is more likely to relax. We observe thus the propagation of a catastrophic event. The hole in the distribution of ages is the consequence of this process. Shear tends to be localized. This process seems robust to us because we have observed it in other simulations not shown here. This issue will be the focus of another manuscript regarding the prediction/behavior of the model.

From the results shown in Figure 15, it is effectively observed that the correlation length increases up to the yield point, from about 1-2 unit lengths (which is about 5-6 nm) up to about 4-5 unit lengths (12-20 nm) at larger deformations, both for glassy and rubbery samples. Thus,

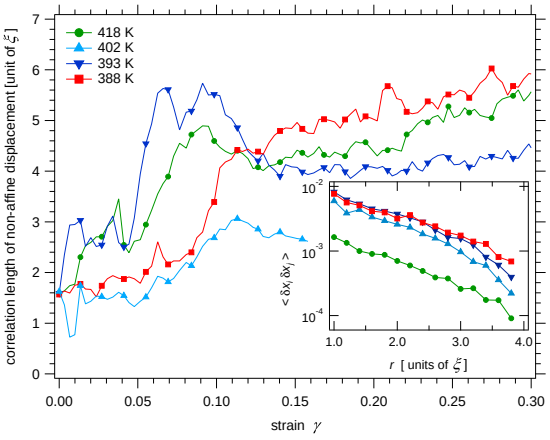

FIG. 15. Correlation length of non-affine displacements for different temperatures. Shear rate is 0.1 s^{-1} and aging time 100 s. The correlation length increases at about 5% deformation from 1-2 up to 4-5 at larger deformations. However, no specific feature of the glassy state can be clearly observed as compared to the rubbery state. Inset: correlation functions of non-affine deformations at different temperatures above and below T_g. The correlation function decreases exponentially. The lower the temperature, the larger the correlation at intermediate distances. The corresponding deformation amplitude is $\gamma = 0.125$.

the increase of the correlation length at and beyond yield is limited to a few units. However, this does not appear to be specific to the yield of glassy polymers since a similar correlation length is observed at temperatures above T_g, even though the average amplitude of the non-affine reorganization is larger at temperatures below T_g than in the rubbery state (see Figure 13). In some instances ($T = 393$ K or 418 K) a maximum is observed in the correlation length at yield. Figure 15 also shows that the behavior of the correlation length is broadly distributed, as a consequence of the small size of our samples. On this scale, each sample exhibits an individual behavior, as we observed also for the velocity profile: the number of shear bands is broadly distributed. This is a general consequence of the disordered nature of the dynamics and mechanical properties of polymers at temperatures close to the glass transition.

VII. CONCLUSION

We have extended a mechanical model that accounts for the dynamical heterogeneities of a polymer glass, and which allows for calculating the mechanical properties of polymers close to and below the glass transition with an Eyring like hypothesis for the local mechanical properties. This is a mesoscale model for which the basic units are the subunits of dynamical heterogeneities. The

stress and strain fields and the dynamical state of each subunit are described at the nanometer scale (3-5 nm). The model, studied by numerical simulation, allows reaching macroscopic time scales. The present study has been focused on describing the non-linear and plastic behavior of glassy polymers close to the glass transition. We have proposed that the elastic energy stored *on the scale of dynamical heterogeneities* effectively reduces the free energy barriers present for internal relaxation. The results we obtain regarding stress-strain curves up to 20% deformation are consistent with known experimental data by assuming that the scale of dynamical heterogeneities are of order 3-5 nm in size. Note that assuming a scale of 1 nm for dynamical heterogeneities (as compared to 5 nm) would result in a yield stress one orders of magnitude smaller. Though this is beyond what we expect regarding the uncertainty of the model, this result cannot constitute an estimate of the scale of dynamical heterogeneities, but is consistent with other estimates [6, 37]. Regarding the temperature range and aging times under study (*i.e.* temperature close to T_g and aging times of order 10^3s), yield appears as the result of an acceleration of the dynamics of subunits with intermediate relaxation times of the same order of magnitude as the time scale of the experiment: consistently with the percolation picture of the model, subunits with very long relaxation times are not affected by the applied deformation. Mechanical loading creates a hole in the distribution of relaxation times at intermediate time scales (around the time scale of the applied deformation for the considered temperatures not very far below T_g). Lee et al [21] and Bending et al [20] have shown that the distribution of relaxation times, as studied by small probe diffusion, gets narrower under stress. More precisely, the so-called Kolhrausch exponent β increases as compared to the system at rest. This effect will be studied in a future work. Our simulations describe the onset of plastic behavior and the reorganization at the scale of dynamical heterogeneities. If glass transition was a real percolation transition, the length scale for microscopic reorganizations at yield should be expected to diverge. Our simulations show that this is not the case: the correlation length of non-affine deformation increases at yield, but do not grow beyond the scale of 10-20 nm: this is a consequence of the continuous nature of the distribution of relaxation times, which smears out percolation effects. Our simulations predict the appearance of shear bands on the scale of about 10 nm at yield and beyond. As discussed in [32], the main features observed with our model seem to be consistent with the results regarding mechanical heterogeneities obtained by molecular dynamics simulations [26, 27, 30]. Further extension of this model will also include microscopic mechanisms responsible for strain hardening, such as those observed by molecular dynamics simulations [67], and studied also by Chen and Schweitzer [43], who have proposed that strain hardening results from anisotropic chain conformations. **The model which has been**

presented here is generic and allows for describing plastic behavior of glassy polymers up to a few tens of percents deformation. We obtain the relevant orders of magnitude for the yield stress as a function of temperature and shear rates or aging time as compared to well known data from literature. The model as it is now will allow for making more detailed and systematic comparisons with experimental data as regard to plastic behavior. In particular, the effect of the width of the relaxation time distributions may be considered since the latter vary by many orders of magnitude, depending on the considered polymers [51]. The width of distribution of relaxation times of glassy polymers may vary between 4 decades to 6 or 7 decades [51], or even more in the case of glassy polymer blends [68, 69]. Detailed comparison between experimental data are made possible by the model as it has been developed here and will be done in future works. We hope that our work will stimulate the study of the whole spectrum of relaxation time during plastic deformation.

VIII. APPENDIX

Simulation parameter	Physical equiv.	Num. value
Thermal energy	k_BT	0.19
Time step dt	10^{-5} s	10^{-5}
Time step subdivision		10
Friction coefficient ζ	(0.2 MPa s)	0.04
Unit length ξ	3 nm	1
Nearest neighbor cutoff	(3.54 nm)	~ 1.18
Excluded volume radius σ	(3 nm)	1
Excluded volume energy u_0	(0.07 k_BT)	0.01
Glassy spring stiffness k_0	$G'_g \sim$ GPa	3000
Plastifying parameter λ	$G'_g\xi/2k_BT \sim$ GPa	1000
Rubbery spring stiffness k_∞	$G'_r \sim$ MPa	0.1
Min. rubbery connectivity		12
Rubbery spring length	(4.5 nm)	1.5
Shear rate	0.1 s^{-1}	0.1
	$C_1 = 9.34$	
WLF parameters	$C_2 = 32.5$ K	
	$T_0 = 393.5$ K	

TABLE I. Table of the main simulation parameters and correspondence with physical quantities.

IX. ACKNOWLEDGMENTS

L. Conca, D. Long and P. Sotta acknowledge support from the FP7-NMP-2011-EU-RUSSIA program CompNanoComp, grant agreement 295355.

[1] Ferry J.D., *Viscoelastic properties of polymers* (John Wiley and Sons, Inc.) **1980**

[2] Ediger M.D., Angell C.A., Nagel S.R., Supercooled liquids and glasses, *J. Phys. Chem* **1996**, *100*, 13200-13212

[3] Ediger M.D., Spatially heterogeneous dynamics in supercooled liquids, *Annu. Rev. Chem.* **2000**, *51*, 99-128

[4] Richert R., Heterogeneous dynamics in liquids: fluctuations in space and time, *J. Phys. : Condens. Matter* **2002**, *14*, R703-R738

[5] Schmidt-Rohr K., Spiess H.W., Nature of Nonexponential Loss of Correlation above the Glass-Transition Investigated by Multidimensional NMR, *Phys. Rev. Lett.* **1991**, *66*, 3020-3023

[6] Tracht U., Wilhelm M., Heuer A., Feng H., Schmidt-Rohr K., Spiess H.W., Length scale of dynamic heterogeneities at the glass transition determined by multidimensional nuclear magnetic resonance, *Phys. Rev. Lett.* **1998**, *81*, 2727-2730

[7] Reinsberg S.A., Qiu X.H., Wilhelm M., Spiess H.W., Ediger M.D., Length scale of dynamic heterogeneity in supercooled glycerol near Tg, *J. Chem. Phys.* **2001**, *114*, 7299-7302

[8] Cicerone M.T., Blackburn F.R., Ediger M.D., Anomalous Diffusion of Probe Molecules in Polystyrene Evidence for Spatially Heterogeneous Segmental Dynamics, *Macromolecules* **1995**, *28*, 8224-8232

[9] Wang C.-Y. and Ediger M.D., Enhanced translational diffusion of 9,10-bis(phenylethynyl)anthracene (BPEA) in polystyrene, *Macromolecules* **1997**, *30*, 4770-4771

[10] Cicerone M.T., Wagner P.A. and Ediger M.D., Translational diffusion on heterogeneous lattices: A model for dynamics in glass forming materials, *J. Phys. Chem.B*, **101** (1997) 8727-8734

[11] Fujara F., Geil B., Sillescu H. and Fleischer G., Translational and Rotational Diffusion in Supercooled Orthoterphenyl Close to the Glass Transition, *Z.Phys.B.*, **88** (1992) 195-204

[12] Hwang Y., Inoue T., Wagner P.A., Ediger M.D., Molecular motion during physical aging in polystyrene: Investigation using probe reorientation, *J. Polym. Sci. , Part B: Polymer Physics* **2000**, *38*, 68-79

[13] Schiener B., Böhmer R., Loidl A., Chamberlin R.V., Nonresonant spectral hole burning in the slow dielectric response of supercooled liquids, *Science* **1996**, *274*, 752-754

[14] Richert R., Triplet state solvation dynamics: Basics and applications, *J. Chem. Phys.* **2000**, *113*, 8404-8229

[15] Nielsen, L.E., Landel R.F., *Mechanical Properties of Polymers and Composites*, (Marcel Dekker, New York) **1994**

[16] Chen K.C., Schweitzer K.S., Microscopic constitutive equation theory for the nonlinear mechanical response of polymer glasses, *Macromolecules* **2008**, *41*, 5908-5918

[17] Chen K., Schweitzer K.S., Stress-enhanced mobility and dynamic yielding in polymer glasses, *Europhys. Lett.* **2007**, *79*, 26006

[18] Loo, L.S.; Cohen, R.E.; Gleason, K.K., Chain mobility in the amorphous region of nylon 6 observed under active uniaxial deformation, *Science* **2000**, *288*, 116-119

[19] Lee H.-N. Riggleman R.A., de Pablo J.J., Ediger M.D., Deformation-Induced Mobility in Polymer Glasses during Multistep Creep Experiments and Simulations, *Macromolecules* **2009**, *42*, 4328-4336

[20] Bending B., Christison K., Ricci J., Ediger M.D., Measurement of Segmental Mobility during Constant Strain Rate Deformation of a Poly(methyl methacrylate) Glass, *Macromolecules* **2014**, *47*, 800-806

[21] Lee H.-N., Paeng K., Swallen S.F., Ediger M.D., Direct Measurement of Molecular Mobility in Actively Deformed Polymer Glasses, *Science* **2009**, *323*, 231-234

[22] Kalfus J., Detwiler A., Lesser A.J. , Probing Segmental Dynamics of Polymer Glasses during Tensile Deformation with Dielectric Spectroscopy, *Macromolecules* **2012**, *45*, 4839-4847

[23] R. Pérez-Aparicio, D. Cottinet, C. Crauste-Thibierge, L. Vanel, P. Sotta, J.-Y. Delannoy, S. Ciliberto, D. R. Long, Dielectric spectroscopy of a stretched polymer glass : heterogeneous dynamics and

plasticity, *Macromolecules* **2016**, *49*, 3889-3898

[24] Hasan O.A., Boyce M.C., Energy-storage during inelastic deformation of glassy-polymers, *Polymer* **1993,** *34*, 5085

[25] Riggleman R.A., Lee H.-N., Ediger M.D., de Pablo J.J., Heterogeneous dynamics during deformation of a polymer glass, *Soft Matter* **2010**, *6*, 287-291

[26] Yoshimoto K., Jain T.S., van Workum K., Nealey P.F., de Pablo J.J., Mechanical heterogeneities in model polymer glasses at small length scales, *Phys. Rev. Lett.* **2004**, *93*, 175501

[27] Leonforte F., Boissière R., Tanguy A., Wittmer J.P., Barrat J.-L., Continuum limit of amorphous elastic bodies. III. Three-dimensional systems, *Phys. Rev. B* **2005**, *72*, 224206

[28] Riggleman R.A., Lee H.-N., Ediger M.D., de Pablo J.J., Riggleman, Robert A. and Lee, H.-N. and Ediger, Mark D. and de Pablo, Juan J., Free volume and finite-size effects in a polymer glass under stress, *Phys. Rev. Lett.* **2007**, *99*, 215501

[29] Tsamados, M.; Tanguy, A.; Goldenberg, C.; Barrat, J.-L., Local elasticity map and plasticity in a model Lennard-Jones glass, *Phys. Rev. E* **2009**, *80*, 026112

[30] Papakonstantopoulos, G.J.; Riggleman R.A., Barrat, J.-L., de Pablo J.J., Molecular plasticity of polymeric glasses in the elastic regime, *Phys. Rev. E* **2008**, *77*, 041502

[31] Riggleman R.A., Schweizer K.S., de Pablo J.J., Nonlinear creep in a polymer glass, *Macromolecules* **2008**, *41*, 4969-4977

[32] Dequidt A., Long D.R., Sotta P., Sanseau O., Mechanical properties of thin confined polymer films close to the glass transition in the linear regime of deformation: Theory and simulations, *Eur. Phys. J. E* **2012**, *35*, 61

[33] Schweizer K.S., Saltzman E.J., Entropic barriers, activated hopping, and the glass transition in colloidal suspensions, *J. Chem. Phys.* **2003**, *119*, 1181-1196

[34] Schweizer K.S., Saltzman E.J., Theory of dynamic barriers, activated hopping, and the glass transition in polymer melts, *J. Chem. Phys.* **2004**, *121*, 1984-2000

[35] Chen K., Schweitzer K.S., Suppressed Segmental Relaxation as the Origin of Strain Hardening in Polymer Glasses, *Phys. Rev. Lett.* **2009**, *102*, 038301

[36] Long D., Lequeux F., Heterogeneous dynamics at the glass transition in van der Waals liquids, in the bulk and in thin films, *Eur. Phys. J E* **2001**, *4*, 371-387

[37] Merabia S., Long D., Heterogeneous dynamics at the glass transition in van der Waals liquids: determination of the characteristic scale, *Eur. Phys. J E* **2002**, *9*, 195-207

[38] Merabia S., Sotta P., Long D., Heterogeneous nature of the dynamics and glass transition in thin polymer films, *Eur. Phys. J E* **2004**, *15*, 189-210

[39] Sotta P., Long D., The cross-over from 2D to 3D percolation. Theory and numerical simulations, *Eur. Phys. J E* **2003**, *11*, 375-388

[40] Ritort F., Sollich P., Glassy dynamics of kinetically constrained models, *Advances in Physics* **2003** *52*, 219-342

[41] Y.-J. Jung, J.P. Garrahan and D. Chandler, Excitation lines and the breakdown of Stokes-Einstein relations in supercooled liquids, Phys. Rev. E **69**, 061205 (2004)

[42] J.P. Garrahan and D. Chander, Geometrical explanation and scaling of dynamical heterogeneities in glass forming systems, Phys. Rev. Lett. **89**, 035704 (2002)

[43] Chen K., Saltzman E.J., Schweizer K.S., Segmental dynamics in polymers: from cold melts to ageing and stressed glasses, *J. Phys. : Condens. Matter* **2009**, *21*, 503101

[44] Adam G., Gibbs J.H., On temperature dependence of cooperative relaxation properties in glass-forming liquids , *J. Chem. Phys.***1965**, *43*, 139

[45] Merabia S., Long D., Heterogeneous dynamics, aging and rejuvenating in van der Waals liquids , *J. Chem. Phys.* **2006**, *125*, 234901

[46] Tito N.B., Lipson J.E.G., Milner S.T., Lattice model of mobility at interfaces: free surfaces, substrates, and bilayers, *Soft Matter* **2013**, *9*, 3173-3180

[47] Baschnagel J., Varnik F., Computer simulations of supercooled polymer melts in the bulk and in-confined geometry, *Journal of Physics-Condensed Matter* **2005**, *17*, R851-R953

[48] Barrat J.L., Baschnagel J., Lyulin A., Molecular dynamics simulations of glassy polymers, *Soft Matter* **2010**, *6*, 3430-3446

[49] Merabia S, Long D., Heterogeneous Dynamics and Pressure Dependence of the Dynamics in van der Waals Liquids, *Macromolecules* **2008**, *41*, 3284-3296

[50] Merabia S., Sotta P. and Long D.R., A Microscopic Model for the Reinforcement and Non-linear Behavior of Filled Elastomers and Thermoplastic Elastomers (Payne and the Mullins effects), *Macromolecules* **2008** *41*, 8252-8266

[51] Masurel R., Cantournet S., Dequidt. A., Long D., Montes H., Lequeux F. , Linear Viscoelasticity of polymer in their glass transition domains : 2d finite elements simulations, *Macromolecules* **2015**, *48*, 6690-6702

[52] De Gennes P.-G., Glass transitions in thin polymer films, *Eur. Phys. J E* **2000**, *2*, 201-203

[53] Eyring H., Viscosity, plasticity, and diffusion as examples of absolute reaction rates, *J. Chem. Phys.* **1936**, *4*, 283-291

[54] Lee H.-N, Paeng K., Swallen S.F., Ediger M.D., Stamm R.A., Medvedev G.A., Caruthers J.M., Molecular Mobility of Poly(methyl methacrylate) Glass During Uniaxial Tensile Creep Deformation, *J. Polym. Sci.: Polym. Phys Ed* **2009** *47*, 1713-1727

[55] Holt D.L., Modulus and yield stress of glassy poly(methyl methacrylate) at strain rates up to 103 inch/inch/second, *Journal of Applied Polymer Science* **1968,** *12*, 1653-1659

[56] Bauwens-Crowet C., Compression yield behavior of polymethyl methacrylate over a wide-range of temperatures and strain-rates, Journal of Materials Science**1973***8*, 968-979

[57] Meijer H.E.H, Govaert L, Mechanical performance of polymer systems: The relation between structure and properties, *Prog. Polym. Sci.* **2005,** *30*, 915-938

[58] Wagner H., Richert R., Dielectric relaxation of the electric field in poly(vinyl acetate): a time domain study in the range 10−3-10^6 s, *Polymer* **1997**, *38*, 255-261

[59] Kremer F., Schonhals A., Broadband Dielectric Spectroscopy, Springer-Verlag, Berlin Heidelberg 2003

[60] Havriliak S., Havriliak S. J., Result from an unbiased analysis of nearly 1000 sets of relaxation data, *J. Non-Cryst. Solids* **1994**, *172*, 297-310

[61] Medvedev G.A. and Caruthers J.M., Development of a stochastic constitutive model for prediction of postyield softening in glassy polymers, J. Rheol. **2013** *57*, 949-1002

[62] Chen K.C., Schweitzer K.S., Theory of Yielding, Strain Softening, and Steady Plastic Flow in Polymer Glasses under Constant Strain Rate Deformation, *Macromolecules* **2011**, *44*, 3988-4000

[63] G. Picard, A. Ajdari, F. Lequeux, L. Bocquet, Slow flows of yield stress fluids: Complex spatiotemporal behavior within a simple elastoplastic model, *Phys. Rev E* **2005,** *71*, 010501

[64] Long, D.; Sotta, P., Numerical simulation for the mesoscale deformation of disoredered and reinforced elastomers, *IMA Volume in Mathematics and its Applications: Modeling of Soft Matter*, Calderer M.-C. T. and Terentjev E.M. Editors **2005,** *141*, 205-234

[65] Long, D.; Sotta, P., Non-linear and Plastic Behavior of Soft Thermoplastic and Filled Elastomers Studied by Dissipative Particle Dynamics, *Macromolecules* **2006,** *39*, 6282-6297

[66] Long, D.; Sotta, P., Slow relaxation in gels, soft thermoplastic elastomers and filled rubbers, *Rheol. Acta* **2007,** *44*, 1029-1044

[67] Hoy R.S., Robbins M.O., Strain hardening of polymer glasses: Entanglements, energetics, and plasticity, *Phys. Rev. E* **2008,** *77*, 031801

[68] Shi, P. L.; Schach, R.; Munch, E.; Montes, H.; Lequeux, F., Glass Transition Distribution in Miscible Polymer Blends: From Calorimetry to Rheology, *Macromolecules* **2013**, *46*, 3611-3620

[69] Peiluo Shi, PhD thesis, ESPCI, Paris **2013**, https://pastel.archives-ouvertes.fr/pastel-00920019/document

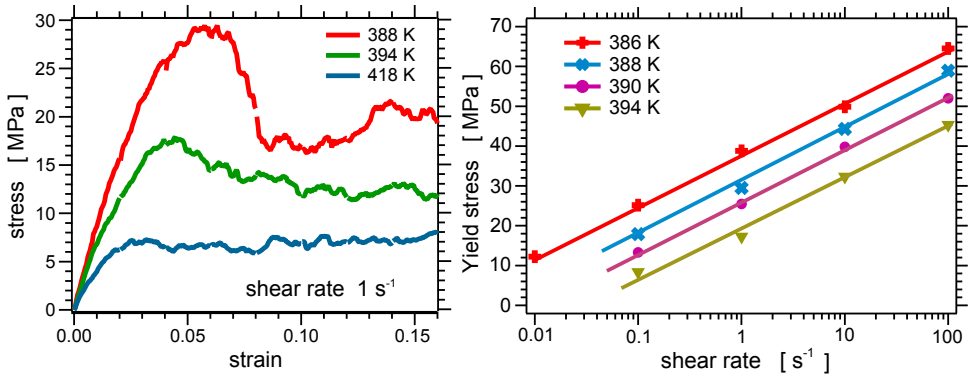

FIG. 16. for TOC only. "Heterogeneous dynamics and polymer plasticity", by Dequidt, Conca, Sotta, Delannoy, Lequeux and Long.